Neurobiology of Disease 213 (2025) 107005

Contents lists available at ScienceDirect

Neurobiology of Disease

journal homepage: www.elsevier.com/locate/ynbdi

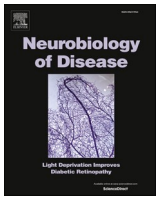

Effect of primary structural variation on cervid prion protein in flexibility, stability, and spontaneous misfolding propensity

Carlos M. Díaz-Domínguez [a,b], Hasier Eraña [a,b,c], Francesca Peccati [a,i], Enric Vidal [d,e], Jorge M. Charco [a,b,c], Cristina Sampedro-Torres-Quevedo [a], Miguel A. Pérez-Castro [a], Nuria L. Lorenzo [f], Samanta Giler [d,e], Glenn C. Telling [g], Mariví Geijo [h], Jesús R. Requena [f], Gonzalo Jiménez-Osés [a,i], Joaquín Castilla [a,b,i,*]

[a] *Center for Cooperative Research in Biosciences (CIC BioGUNE), Basque Research and Technology Alliance (BRTA), Derio, Spain.*
[b] *Centro de Investigación Biomédica en Red de Enfermedades infecciosas (CIBERINFEC), Carlos III National Health Institute, Madrid, Spain.*
[c] *ATLAS Molecular Pharma S. L., Derio, Spain.*
[d] *IRTA. Programa de Sanitat Animal. Centre de Recerca en Sanitat Animal (CReSA), Campus de la Universitat Autònoma de Barcelona (UAB), Bellaterra, Catalonia. Spain.*
[e] *Unitat mixta d'Investigació IRTA-UAB en Sanitat Animal. Centre de Recerca en Sanitat Animal (CReSA), Campus de la Universitat Autònoma de Barcelona (UAB), Bellaterra, Catalonia. Spain.*
[f] *CIMUS Biomedical Research Institute & Department of Medical Sciences, University of Santiago de Compostela-IDIS, Santiago de Compostela, Spain.*
[g] *Prion Research Center. Colorado State University, Fort Collins, USA.*
[h] *Animal Health Department, NEIKER-Basque Institute for Agricultural Research and Development, Basque Research and Technology Alliance (BRTA), Derio, Spain.*
[i] *Ikerbasque, Basque Foundation for Science, Bilbao, Spain.*

A R T I C L E I N F O

Keywords:
CWD
Misfolding
Polymorphisms
Prion
Proteinopathy
Stability
Structure

A B S T R A C T

Protein misfolding is central to numerous neurodegenerative disorders, collectively known as proteinopathies, which include Alzheimer's disease, Parkinson's disease, and prion diseases, among others. In many cases, specific polymorphisms of the proteins associated with these diseases influence their misfolding. However, the precise ways in which these polymorphisms affect protein integrity and how they contribute to misfolding propensity remain unclear. In the case of prion diseases, they are caused by prions or PrP^{Sc}, the misfolded isoforms of the cellular prion protein (PrP^{C}). Chronic Wasting Disease (CWD) is a prion disease that affects cervids and can exhibit lymphotropic properties, making it the most widespread proteinopathy. For that reason, cervid PrPs and their polymorphisms have been extensively studied. To better understand the role of these polymorphisms, we analyzed 45 cervid PrP variants to assess their effects on flexibility, stability, and spontaneous misfolding propensity.

The cervid variants were expressed as recombinant PrP in *E. coli* and were analyzed for thermal stability using circular dichroism. Additionally, the rec-PrPs served as substrates for Protein Misfolding Shaking Amplification

Abbreviations: TSE, Transmissible Spongiform Encephalopathies; PrP, Prion Protein; PrP^{C}, Cellular Prion Protein; PrP^{Sc}, Scrapie-associated Prion Protein; CWD, Chronic Wasting Disease; NA, North America; CNS, Central Nervous System; PMCA, Protein Misfolding Cyclic Amplification; rec, Recombinant; rec-PMCA, Recombinant Protein Misfolding Cyclic Amplification; PMSA, Protein Misfolding Shaking Amplification; MD, Molecular Dynamics; PCR, polymerase chain reaction; Tris-HCl, [tris(hydroxymethyl)aminomethane hydrochloride]; PMSF, phenylmethylsulfonyl fluoride; ACS, sodium phosphate dibasic anhydrous; BCA, Bicinchoninic Acid; CB, Conversion Buffer; CD, Circular Dichroism; Cs_2SO_4, Cesium Sulfate; DE3, λDE3 Lysogen in *E. coli*; DNase, Deoxyribonuclease; EDTA, Ethylenediaminetetraacetic Acid; IPTG, Isopropyl β-D-1-thiogalactopyranoside; LB, Luria-Bertani broth; NaCl, Sodium Chloride; PBS, Phosphate-Buffered Saline; DPBS, Dulbecco's Phosphate-Buffered Saline; PK, Proteinase K; PrP^{res}, Protease-Resistant Prion Protein; SDS-PAGE, Sodium Dodecyl Sulfate Polyacrylamide Gel Electrophoresis; RMSD, Root Mean Square Deviation; FF, Fraction Folded; SHAKE, Algorithm for molecular dynamics simulations; *E*, ellipticity values; T_m, Melting Temperature; Δ*H*m, enthalpy of unfolding at the melting temperature; Δ*C*p, change in specific heat capacity of unfolding; VMD, Visual Molecular Dynamics; S, spontaneous misfolding propensity score; GFAP, glial fibrillary acidic protein; Pfc, piriform cortex; H, hippocampus; Oc, occipital cortex; Tc, temporal cortex; Pc, parietal cortex; Fc, frontal cortex; S, striatum; T, thalamus; HT, hypothalamus; M, mesencephalon; Mobl, medulla oblongata; Cm, cerebellar nuclei; Cv, cerebellar vermis; Cc, cerebellar cortex; ORF, open reading frame; pLDDT, predicted Local Distance Difference Test; RMSF, per-residue root mean square fluctuations; vCJD, Variant Creutzfeldt-Jakob disease; Δ*G*u, free energy of unfolding..

* Corresponding author at: Center for Cooperative Research in Biosciences (CIC BioGUNE), Basque Research and Technology Alliance (BRTA), Derio, Spain.
E-mail address: jcastilla@cicbiogune.es (J. Castilla).

https://doi.org/10.1016/j.nbd.2025.107005
Received 10 April 2025; Received in revised form 26 May 2025; Accepted 12 June 2025
Available online 13 June 2025

(PMSA), enabling assessment of each variant's spontaneous misfolding propensity. This process led to the formation of *bona fide* prions, as confirmed by inoculation of one of the resulting conformers into transgenic mice expressing bank vole PrP. In parallel, molecular dynamics simulations were conducted to analyze the structural flexibility of the variants. While differences in protein flexibility were observed, no correlation was detected among flexibility, thermal stability, and the observed variable spontaneous misfolding propensity, suggesting that these properties are independent parameters.

1. Background

Transmissible Spongiform Encephalopathies (TSE), or prion diseases, comprise a group of rare and fatal neurological disorders that affect humans and other mammals (Prusiner, 1998). The underlying cause of these diseases is the PrP^{Sc} or prion, an abnormal isoform of the physiological prion protein, PrP^{C}. PrP^{C} is a globular protein rich in α-helix domains, soluble, susceptible to protease digestion, and non-neurotoxic. Conversely, PrP^{Sc} is a fibrillary protein rich in β-sheet domains, insoluble, partially resistant to protease digestion, and neurotoxic, which also has the ability to recruit and convert PrP^{C} monomers through a yet poorly characterized misfolding and propagation process (Colby and Prusiner, 2011). In addition to the PrP^{Sc}-induced or template misfolding, spontaneous misfolding of PrP^{C} can also occur (Hill et al., 2003).

One of the most concerning TSEs today is Chronic Wasting Disease (CWD). CWD has been detected in different species of both captive and free-ranging cervids. It is widespread in North America (NA), affecting 31 states in the United States and 4 provinces in Canada, with related cases also reported in South Korea (Benestad and Telling, 2018). In 2016, new cases were reported in distinct cervid species in Norway, followed by others in Sweden and Finland (Benestad et al., 2016; Pirisinu et al., 2018; Vikoren et al., 2019). Further analysis of these cases revealed that they were caused by prion strains different than NA CWD, confirming that they were unrelated (Bian et al., 2021; Nonno et al., 2020). One of the most significant features of NA CWD is its extensive horizontal transmission capacity, which is mainly facilitated by the presence of prions in excreted fluids and peripheral tissues of affected animals (Moreno and Telling, 2018). Although differing in other respects, the prion strain found in Norwegian reindeer shared this characteristic with NA CWD (Bian et al., 2021; Nonno et al., 2020). In contrast, the Nordic strains discovered in moose and red deer appear to have a more limited horizontal transmission potential (Tranulis, 2021), which could be partially attributed to PrP^{Sc} being predominantly restricted to the central nervous system (CNS) of the animals (Sola et al., 2023). Moreover, the advanced age of the affected Nordic moose and red deer, as well as the unusual biochemical pattern of the PrP^{Sc} detected in their CNS, suggests that this form of CWD could have a spontaneous origin (Tranulis, 2021).

In this context, some polymorphisms identified within the cervid PrP^{C} modulate its misfolding propensity and the susceptibility of these animals to disease (Arifin et al., 2021). Importantly, the influence of all these variants in prion propagation and transmission has been assessed through *in vitro* experiments and bioassays involving transgenic mice expressing them, confirming their protective effects against NA CWD (Bartz et al., 2024). Many of the *in vitro* experiments were conducted using the Protein Misfolding Cyclic Amplification (PMCA) technique, which, by employing PrP^{C} present in brain homogenates as a substrate, mimics the natural misfolding process but at an accelerated rate (Saa et al., 2005). PMCA not only replicates the effect of the variants in terms of susceptibility or resistance to NA CWD-induced misfolding but also allows the analysis of dominant negative effects, as observed in the case of the S138N variant when expressed in the heterozygosis state (Arifin et al., 2023).

In light of the high variability among the Nordic CWD cases and their potential spontaneous origin (Tranulis, 2021), further studies analyzing the effects of variants of cervid PrP^{C}, not only on CWD transmission but also on spontaneous misfolding, are necessary. While most *in vitro* CWD research focuses on the impact of PrP^{C} variants on propagation (Pritzkow, 2022), strain characterization (Otero et al., 2023), and prion detection in different tissues, fluids, and materials (Bartz et al., 2024), only one study has addressed the spontaneous misfolding of cervid PrP^{C} (Meyerett-Reid et al., 2017). Using brain homogenate from transgenic mice overexpressing elk PrP^{C} (Tg5037), this study achieved spontaneous misfolding after four serial rounds of PMCA. Nonetheless, relying on transgenic mouse brain homogenates limits large-scale studies of different PrP^{C} variants. However, this limitation can be overcome by the latest developments on recombinant (rec) PrP misfolding and *in vitro* handling. Similar to standard PMCA, rec-PMCA has demonstrated versatility in studying transmission barriers, identifying key amino acids, analyzing cofactor effects on resulting recombinant prions, and inducing spontaneous rec-PrP misfolding (Kim et al., 2010).

Inspired by rec-PMCA and other precursor *in vitro* prion generation methods, our laboratory has developed Protein Misfolding Shaking Amplification (PMSA), a technique capable of inducing the misfolding of rec-PrP through the propagation of a preformed seed (Erana et al., 2019) or *via* spontaneous misfolding (Eraña et al., 2023). In both scenarios, this process results in the formation of *bona fide* prions able to cause a prion disease in animal models. Originally optimized using bank vole rec-PrP due to its remarkable spontaneous misfolding capacity, we have proven that PMSA has the potential to promote the spontaneous misfolding of most PrP variants from mammals known so far (Erana et al., 2024). This makes PMSA a perfect tool to evaluate the spontaneous misfolding proneness of the different cervid PrP variants.

Additionally, the presence of amino acid changes could alter certain protein properties, such as stability and flexibility. However, "stability" is a broad term that encompasses various properties, including thermal stability, resistance to degradation, and resistance to oxidation. In this study, we specifically focus on thermal stability as an experimentally measurable parameter. While it has been suggested that protein stability and prion misfolding are inversely correlated (Weissmann, 2004), we previously reported no apparent correlation between computationally predicted thermal stability changes and spontaneous misfolding (Erana et al., 2024). Experimental analysis of these parameters using cervid PrP variants could definitively determine whether a correlation exists. Using PMSA, we assessed the spontaneous misfolding proneness of over 40 different cervid PrP variants found in nature. Thermal stability was experimentally determined by circular dichroism, and molecular dynamics (MD) simulations were employed to evaluate flexibility and structural properties. Remarkably, our data show that nearly all the cervid PrP variants, despite exhibiting similar thermal stability, have the ability to generate a wide variety of *bona fide* infectious prions. This suggests that misfolding propensity appears to be largely independent of thermal stability under our experimental conditions, underscoring the remarkable versatility of this highly polymorphic protein to adopt misfolded structures with unknown zoonotic potential. These findings are particularly significant given the current situation in Europe, where the identification of CWD cases distinct from those in NA outlines an unpredictable scenario in which these variants could play a relevant role.

2. Methods

2.1. Recombinant prion protein expression and purification

The expression and purification of the 45 recombinant PrP utilized in this study was conducted following previously established protocols (Erana et al., 2023). Briefly, the rec-PrP sequences, spanning amino acids 23 to 234 in the cervid reference PrP numbering (Q226Q, GenBank Accession Number AYY330343), were either obtained from species genomic DNA *via* PCR or synthesized (NzyTech and GeneScript). These sequences were cloned into the pOPIN E expression vector, a construct developed by Oxford Protein Production Facility UK (OPPF). Upon transformation into *E. coli* Rosetta™ (DE3) competent cells (EMD Millipore), they were grown in LB broth containing ampicillin, and the induction of recombinant protein expression was done using isopropyl β-D-1-thiogalactopyranoside (IPTG) (Gold biotechnology). Following bacterial lysis, which was done using a buffer containing 50 mM tris (hydroxymethyl)aminomethane hydrochloride (Tris-HCl) (Fisher Bioreagents), 5 mM ethylenediaminetetraacetic acid (EDTA) (Sigma-Aldrich), 1 % Triton X-100 (Sigma-Aldrich), 1 mM phenylmethylsulfonyl fluoride (PMSF) (Sigma-Aldrich), 100 μg/ml lysozyme (Sigma-Aldrich), 100 U/ml deoxyribonuclease (DNase) (Sigma-Aldrich), 20 mM $MgCl_2$ (Sigma-Aldrich), pH 8, inclusion bodies were solubilized using a buffer containing 20 mM Tris-HCl (Fisher Bioreagents), 0.5 M NaCl (Sigma-Aldrich), 6 M guanidine-HCl (Fisher Scientific), pH 8. Purification of the rec-PrP was achieved through immobilized metal affinity chromatography utilizing His-trap columns (HisTrap FF crude 5 ml, Cytiva). After centrifugation (8500 *g* for 15 min at 4 °C), the clarified cell extract was loaded onto the column, washed, and eluted using a buffer containing 20 mM Tris-HCl, 500 mM NaCl (Sigma-Aldrich), 500 mM imidazole (Sigma-Aldrich), and 2 M guanidine-HCl, pH 8. Post-elution, the guanidine-HCl concentration was increased to 6 M for long-term storage at −80 °C. Subsequently, the protein concentration was adjusted to 25 mg/ml utilizing centrifugal filter units (Amicon® Ultra-15 PLGC Ultracel-PL 10 KDa, Millipore), and a *Nanodrop 2000* (Fisher Scientific) for absorbance measurements at 280 nm. Finally, protein quantity and purity were assessed through methanol precipitation, electrophoresis on SDS-PAGE gels (BioRad), and total protein staining (BlueSafe, Nzytech).

2.2. AlphaFold structure prediction

The structures of the 27 PrP^C prion variants (residues 132–229) were predicted using AlphaFold 2.3.2 (Jumper et al., 2021) using the following options:

–db-preset = reduced_dbs.
–model-preset = monomer.
–max-template-date 2050-01-01.
–enable-gpu-relax.
–models-to-relax all.

For each sequence 10 independent predictions were run using different seeds and the training parameters corresponding to model 3 (Jumper et al., 2021).

2.3. Molecular dynamics (MD) simulations

MD simulations were carried out with the AMBER 22 (Case et al., 2023) suite using the ff19SB force field (Tian et al., 2020). For each cervid prion sequence, the structure with the highest prediction confidence (pLDDT score) was used as the starting geometry. Proteins were immersed in a water box with a 10 Å buffer of OPC3 water molecules (Izadi and Onufriev, 2016) and neutralized by adding explicit Na^+ counterions (Li-Merz 12–6 nonbonded model (Li et al., 2015)). A two-stage geometry optimization approach was implemented. The first stage minimizes only the positions of solvent molecules and ions, and the second stage is an unrestrained minimization of all the atoms in the simulation cell. The systems were then heated by incrementing the temperature from 0 to 300 K under a constant pressure of 1 atm and periodic boundary conditions. Harmonic restraints of 10 kcal mol^{-1} $Å^{-2}$ were applied to the solute, and the Andersen temperature coupling scheme (Andersen, 1980) was used to control and equalize the temperature. The time step was kept at 1 fs during the heating stages, allowing potential inhomogeneities to self-adjust. The SHAKE (Miyamoto and Kollman, 1992) algorithm was employed for further equilibration and production with a 2 fs time step. Long-range electrostatic effects were modelled using the particle mesh Ewald method (Darden et al., 1993). A cutoff of 8 Å was applied to Lennard-Jones interactions. Each system was equilibrated for 2 ns at constant volume and temperature of 300 K. Production was run as a single 1 μs simulation at constant volume and temperature of 300 K, with no restraints. RMSD and atomic fluctuation analyses were carried out with cpptraj (Roe and Cheatham 3rd, 2013). Secondary structure analysis was carried with VMD 1.9.3. (Humphrey et al., 1996).

2.4. Determination of melting temperatures for rec-PrP by circular dichroism

The melting temperatures (T_m) of cervid rec-PrP variants were determined *via* circular dichroism (CD). The purified rec-PrP samples were diluted at a ratio of 1:5 in a sodium phosphate buffer [10 mM sodium phosphate dibasic anhydrous (ACS), pH 5.8] and dialyzed for 1 h at room temperature (20–22 °C) against the same buffer to remove guanidine-HCl present in the sample. This process effectively reduced the guanidine-HCl concentration by approximately 1:1000,000 while retaining the protein concentration. Post-dialysis, the rec-PrP solutions were centrifuged at 19,000 *g* for 15 min at 4 °C to eliminate protein aggregates. The resulting supernatant was then diluted in the sodium acetate buffer to reach a concentration of 0.03 mg/ml, as confirmed by a protein quantification assay (bicinchoninic acid, BCA assay, Thermo Scientific). Samples were then loaded into 5 mm quartz cuvettes (Macro cell 100-QS, 5 mm; Hellma Analytics) and ellipticities were recorded a fixed wavelength (222 nm) and a temperature range from 20 to 90 °C using a Jasco J-810 spectropolarimeter coupled to a Peltier temperature control unit.

For each variant, T_m values were determined by fitting ellipticity values (E) against temperature using a two-state (folded/unfolded) model. The fitting process involved a least-squares minimization of the error between the measured ellipticity values E and the simulated ellipticity values E_{sim}. The simulation utilized the equation:

$$E_{sim} = FF_{sim}(m_1 T + b_1) + (1 - FF_{sim})(m_2 T + b_2)$$

where FF_{sim} represents the fraction of protein in the native (folded) state, T is the temperature, and the parameters m_1, b_1, m_2, and b_2 denote the slopes and intercepts of the (linear) ellipticity in the native and denatured state, respectively. FF_{sim} is defined as a parametric function where ΔH_m (the enthalpy of unfolding at the melting temperature) and T_m are the parameters to optimize, and ΔC_p, the change in specific heat capacity of unfolding, is a constant. ΔC_p is estimated based on the number of residues. The initial guess values for ΔH_m and T_m were set to 200 kJ mol^{-1} and 333.15 K (60 °C), respectively. Initial guesses of m_1, b_1, m_2, and b_2 were obtained from linear fitting of the first 20 ellipticity points (m_1, b_1) and the last 20 ellipticity points (m_2, b_2).

2.5. Substrate preparation for protein misfolding shaking amplification

PMSA substrates for spontaneous rec-PrP^{res} formation were prepared as previously described (Erana et al., 2024). Briefly, the purified rec-PrP was diluted 1:5 in phosphate buffered saline (PBS, Hyclone), dialyzed against PBS at 1:2000 ratio for 1 h at room temperature, and centrifuged at 19,000 *g* for 15 min at 4 °C to eliminate amorphous aggregates. The resulting supernatant was further diluted in conversion buffer (CB)

(Eraña et al., 2023) at a ratio of 1:9. Dextran sulphate sodium salt from *Leuconostoc spp.*, with molecular weights ranging from 6500 to 10,000 (Sigma-Aldrich), was added to a final concentration of 0.5 % (*w/v*). All substrates were aliquoted and stored at −80 °C.

2.6. Protein misfolding shaking amplification

To induce spontaneous misfolding of the rec-PrP variants, the Protein Misfolding Shaking Amplification (PMSA) methodology presented recently (Erana et al., 2024) was followed. In summary, the previously prepared substrates were divided and placed into eight 2 ml tubes with conical bottoms and screw caps (Fisherbrand). Four of those tubes were supplemented with 100 mg of glass beads with a diameter of 0.1 mm (BioSpec Products, Inc.), while the remaining four received 100 mg of glass beads with a diameter of 1 mm (BioSpec Products, Inc.). The resulting tubes underwent PMSA at 39 °C using a Digital Shaking Dry-bath (ThermoScientific) equipped with internal temperature control, subject to continuous shaking at 700 rpm for 24 h. Successive PMSA rounds, of 24 h each, were performed for each substrate. In each round, the PMSA product from the preceding cycle was diluted at a ratio of 1:10 into a new set of eight tubes containing freshly thawed substrate and their corresponding beads.

2.7. Misfolded, protease-resistant recombinant PrP (rec-PrP^{res}) detection

All PMSA products from the four serial rounds were transferred from the reaction tubes to 1.5 ml Eppendorf tubes. Enzymatic digestion was done using proteinase K (PK) (Roche) at a concentration of 25 μg/ml and incubating the samples for 1 h at 42 °C in a laboratory oven (Nahita). Subsequently, samples were centrifuged at 19,000 *g* at 4 °C for 15 min, discarding the supernatant after that. The pellets were then resuspended and washed with 750 μl of PBS (Fisher Bioreagents). Finally, samples were centrifuged for another 15 min at 19,000 *g* and 4 °C, followed by resuspension of the pellets in 15 μl of 4× loading buffer (NuPage LDS, Invitrogen), which had been pre-diluted to 1× in PBS.

PK-digested samples were boiled for 10 min at 100 °C and loaded onto 4–12 % acrylamide gels (NuPAGE Midi gel, Invitrogen Life Technologies), running the electrophoresis for 1 h and 20 min (10 min at 70 V, 10 min at 110 V and 1 h at 150 V). PK-resistant PrP detection was done through total protein staining with BlueSafe (NZYTech) for 1 h at room temperature.

2.8. Scoring the spontaneous misfolding propensity

In order to rank the spontaneous misfolding propensity of the 45 cervid rec-PrP analyzed in this study, a previously devised formula was used (Erana et al., 2024). This formula scores the spontaneous misfolding capacity of PMSA-submitted rec-PrP considering different parameters:

$$S_{0.1mm} = 0.4*(n1*10 + n2*6 + n3*3 + n4*1)$$

$$S_{1mm} = 1*(n1*10 + n2*6 + n3*3 + n4*1)$$

$$S = \frac{(S_{0.1mm} + S_{1mm})}{112}*100$$

where n is the number of rec-PrP^{res} positive tubes, the numeric subindexes indicate the PMSA round (from 1 to 4), and $S_{0.1mm}$ and S_{1mm} representing, therefore, the scores obtained for replicates complemented with 0.1 mm diameter and 1 mm diameter glass beads, respectively. The tube sets containing beads of different sizes were assigned different values. Specifically, contribution to the final misfolding score (S) of the replicates complemented with 0.1 mm diameter beads was lower than that assigned to replicates with 1 mm diameter beads. This differentiation was based on prior observations that suggested rec-PrP^{res} misfolding was not solely influenced by the presence of a specific glass surface but was also strongly affected by bead movement (Eraña et al., 2023; Erana et al., 2024). Consequently, tubes supplemented with 1 mm diameter glass beads were found to be more restrictive in terms of inducing spontaneous misfolding of rec-PrP. As a result, a higher value was assigned to these positive tubes compared to those supplemented with 0.1 mm beads.

2.9. Generation of synthetic cervid images

All the cervid images used in the PrPdex files were generated using the DALL-E3 model as implemented in GPT-4o.

2.10. Transmission electron microscopy

Approximately 20 ml of PMSA product containing Deer-D-Dx rec-PrP^{res} underwent digestion with PK at 25 μg/ml and 42 °C for 1 h. The resulting product was concentrated 10× by sedimentation, reducing the total volume to 2 ml. These concentrated sample was washed twice with phosphate-buffered saline (PBS, Hyclone) centrifuging at 19,000 *g* for 15 min each time. The pellet was then resuspended in 2 ml of PBS.

This product was then placed in a Thinwall Ultra-Clear, 13.2 ml, centrifuge tube (Beckman Coulter) on top of a continuous Cs2SO4 gradient ranging from 1 M to 1.7 M, previously prepared with a gradient mixer (Sigma-Aldrich). The sample was ultracentrifuged using a SW41 Ti Swinging bucket rotor (Beckman Coulter) at 210,000 *g* for 15 h at 20 °C. The fractions resulting from this process were examined for the detection of a visible precipitated halo, which was transferred to a 2 ml Eppendorf tube and diluted with the maximum volume of PBS. After centrifugation at 19,000 *g* for 15 min, the pellet was washed with 1 ml of PBS and centrifuged again, repeating the washing steps three times. Finally, the purified fraction, was resuspended in 50 μl of PBS.

Following sonication in a cup horn sonicator (S700, Qsonica) at 80 % power for 2 min (4 pulses of 30 s), the sample was deposited on freshly glow-discharged carbon-coated copper grids (Carbon Film 400 Mesh, Cu) (Electron Microscopy Sciences). The grids were washed with de-ionized H_2O and stained with freshly prepared, filtered 5 % uranyl acetate solution. Imaging was conducted on a JEM-2200FS/CR (JEOL Europe, Croissy-sur-Seine, France) transmission electron microscope equipped with a field emission gun (FEG) operated at 200 kV.

2.11. Determination of infectivity of the rec-PrP^{res} generated by PMSA

To assess the potential of the selected rec-PrP^{res} to induce a TSE in animals, we challenged transgenic mice expressing the prion protein from bank voles (*Myodes glareolus*) with the I109 polymorphism (GenBank accession number AF367624) at a 1-fold concentration. In the first passage, the inoculum was prepared by diluting the selected PMSA product at a 1:10 ratio in sterile DPBS (Invitrogen). For the second passage, a brain-derived inoculum was prepared by homogenizing the brain of one of the diseased animals at 10 % (*w/v*) in DPBS with a protease inhibitor cocktail (PI, Roche), and further diluting it at a 1:10 ratio in DPBS, resulting in a final 1 % brain homogenate. Intracerebral inoculations were administered to groups of 6–8 TgVole 1× mice, with each mouse receiving 20 μl of the inoculum through a sterile disposable 27-gauge hypodermic needle under gaseous anaesthesia (Isoflurane, IsoVet®, Braun). Mice were provided *ad libitum* access to food and water, and underwent examination at least twice a week, turning daily upon the development of neurological signs of disease. The monitored clinical signs included kyphosis, gait abnormalities, altered coat state, depressed mental state, flattened back, eye discharge, hyperactivity, loss of body condition, and incontinence. Animals displaying two or more severe signs or debilitating motor disturbances were euthanized before neurological impairment compromised their welfare. Euthanasia was performed through exposure to a rising concentration of carbon dioxide or, alternatively, by cervical dislocation. Survival time, measured in days post inoculation (dpi), was calculated as the interval between

inoculation and sacrifice. Brains from all inoculated animals were harvested and sagittally divided, with one half fixed in formalin and the other half stored at −80 °C for subsequent anatomopathological and biochemical analysis, respectively. TgVole 1× mice were bred at CIC bioGUNE (Spain) and inoculated at Neiker - Basque Institute for Agricultural Research and Development and at Centro de Biomedicina Experimental (CEBEGA) - University of Santiago de Compostela, registered in the Spanish Register of breeding, supplier and user centers with the number ES150780292901. All experiments adhered to the guidelines outlined in the Spanish law "Real Decreto 53/2013 de 1 de febrero" on the protection of animals used for experimentation and other scientific purposes, based on the European Directive 2010/63/UE on Laboratory Animal Protection. The project received approval from the Ethical Committees on Animal Welfare (project code P-CBG-CBBA-0519 at CIC bioGUNE, NEIKER-OEBA-2021-003 at Neiker, and permit 15005/16/006 at CEBEGA) and was conducted under their supervision.

2.12. PrP^{Sc} detection in brains of inoculated animals

To verify the manifestation of *bona fide* prion disease in inoculated animals, the presence of protease-resistant, misfolded PrP (PrP^{Sc}) was assessed in brain homogenates of deceased subjects. To achieve this, 10 % brain homogenates were mixed at a 1:1 (*v*/v) ratio with digestion buffer [2 % (w/v) Tween-20 (Sigma-Aldrich), 2 % (v/v) NP-40 (Sigma-Aldrich), and 5 % (w/v) Sarkosyl (Sigma-Aldrich) in PBS]. Subsequently, the mixture underwent digestion with PK (Roche) at a concentration of 85 μg/ml and a temperature of 56 °C for 1 h with moderate shaking (450 rpm). The digestion process was halted by adding loading buffer (NuPage 4× Loading Buffer, Invitrogen) at a 1:3 (v/v) ratio, followed by boiling the samples for 10 min at 100 °C. The digested samples were loaded onto 4–12 % acrylamide gels (NuPAGE Midi gel, Invitrogen Life Technologies) and run for approximately 1 h and 20 min. After transferring the gel to PVDF membranes (Trans-Blot Turbo Transfer Pack, Bio-Rad) using the Trans-Blot® TurboTM transfer system (Bio-Rad), the membranes were blocked by incubation in 5 % non-fat milk powder for 1 h at room temperature. For the primary antibody, the membranes were incubated for 1 h at room temperature with Sha31 (Bertin Bioreagents) at a dilution of 1:4000 in 2 % (w/v) Tween-20 with 0.1 % non-fat milk powder (Sigma-Aldrich) in PBS. Following three washes with washing buffer [2 % (w/v) Tween-20 in PBS], a peroxidase-conjugated secondary goat anti-human IgG [H + L, Thermo Scientific or anti-mouse antibody (m-IgGκ BP-HRP, Santa Cruz Biotechnology)] antibody was added at a 1:3000 dilution in the same buffer as the primary antibody, incubating the membranes for 1 h at room temperature. Finally, after three additional washes, the membranes were developed with an enhanced chemiluminescent horseradish peroxidase substrate (West Pico Plus, Thermo Scientific), using iBright 750 (Thermo-Scientific) for image acquisition and AlphaView (Alpha Innotech) software for image processing.

2.13. Anatomopathological analysis and immunohistochemistry

Transversal sections of the half-brains, fixed with a 10 % solution of phosphate-buffered formalin, underwent dissection at the levels corresponding to the medulla oblongata, piriform cortex, and optic chiasm. After dehydration through a gradient of alcohol concentrations and xylene, the samples were embedded in paraffin-wax (Eraña et al., 2023). Four-micrometer sections were mounted on glass microscope slides and subjected to hematoxylin and eosin staining for morphological evaluation.

For immunohistochemistry, additional sections were mounted on glass slides coated with 3-triethoxysilylpropylamine. The immunohistochemical detection of PrP^{res} followed a previously established protocol (Siso et al., 2004). In brief, deparaffinized sections underwent epitope unmasking treatments involving immersion in formic acid, boiling at low pH (6.15) in a pressure cooker, and pre-treatment with PK (4 μg/ml, Roche). Endogenous peroxidases were blocked by immersion in a 3 % H_2O_2 in methanol solution. Then, the sections were incubated overnight with the anti-PrP monoclonal antibody 6C2 (1:1000, CVI-Wageningen UR). Visualization was achieved using the Goat anti-mouse EnVision system (DAKO) and 3,3′-diaminobenzidine (Sigma Aldrich) as the chromogen substrate. Omission of the primary antibody served as a background control. For the astrocyte immunostaining, a rabbit polyclonal antibody against glial fibrillary acidic protein (GFAP, 1:400, DAKO) was used, after heat induce epitope retrieval with citrate buffer (pH 6.0).

Histological evaluation of brain lesions, specifically spongiform changes, and PrP^{res} immunolabeling were conducted by a single pathologist using a light microscope. A semi-quantitative approach, as previously described (Vidal et al., 2015), was employed. Scores ranging from (0) denoting the absence of spongiosis or immunolabeling to (4) indicating maximum intensity of lesion or immunolabeling were assigned to each of the fourteen brain regions studied. These regions included the piriform cortex (Pfc), hippocampus (H), occipital cortex (Oc), temporal cortex (Tc), parietal cortex (Pc), frontal cortex (Fc), striatum (S), thalamus (T), hypothalamus (HT), mesencephalon (M), medulla oblongata (Mobl), cerebellar nuclei (Cm), cerebellar vermis (Cv), and cerebellar cortex (Cc). Brain profiles were plotted as a function of the anatomical areas which were ordered along the horizontal axis to represent the caudo-rostral axis of the encephalon. Graphs were plotted using Microsoft Office Excel software.

3. Results

3.1. Production of the recombinant versions of different variants of cervid PrP

A total of 59 different variants of PrP were identified within species from the Cervidae family. Table 1 lists all these variants along with their GenBank ID (when available), the host animal in which they were described, and the article first citing them. The cervid PrP most frequently found in nature (GenBank ID AY330343), prevalent in genera such as *Odocoileus*, *Alces*, and *Rangifer*, has been selected as the reference sequence and is referred to as Q226Q. Other variants are named by comparing their sequences with the reference.

Although 61 variants were initially identified, only variants with polymorphisms located in the protease-resistant core of the prion after misfolding (residues 90–233) were selected. For those cases in which a variant has multiple polymorphisms in both the flexible region and the protease-resistant core of the prion, only the amino acid changes in the region of interest were considered. Thus, from the initial 61 variants, 47 different plasmids were generated to produce the recombinant versions of these prion proteins in *Escherichia coli* (residues 23–233).

To achieve this, the open reading frames (ORFs) of each *PRNP*, encoding PrP from amino acid 23 to the C-terminus, were obtained either from genomic DNA extracted from biological specimens or through synthesis. These ORFs were cloned into the pOPIN E vector and expressed in *E. coli*. After purification, all proteins were concentrated to 25 mg/ml and supplemented with 6 M guanidine for long-term storage. For their use in either thermostability assays or as substrates for PMSA, purified rec-PrP underwent dialysis. Depending on the purpose of the dialyzed proteins, further folded protein concentration adjustment was required, assessed either by a protein quantification assay or through electrophoresis and total protein staining.

The expression yield of two variants that feature introduction of an extra cysteine (G96C A123T N176D Q226Q and S225C Q226Q) was notably lower than for the other variants, likely a consequence of formation of aberrant disulfide bonds during refolding, so they could not be included in the subsequent experiments. Thus, a total of 45 different substrates were prepared.

Table 1
Polymorphic cervid PrP variants: species of first description, GenBank accession numbers, and references.

Polymorphic variant	Species where firstly described	GenBank ID (Accession number)	Reference
G7C Q226Q[#]	Mule deer	QMT15196[+]	(Zink et al., 2020)
V15A Q226Q[#]	Red deer	FJ436713	(Peletto et al., 2009)
D20G Q226Q[#]	Mule deer	QKI86691	(Wilson et al., 2009)
T36N Q226Q[#]	Moose	Not available	(Wik et al., 2012)
G37V Q226Q[#]	White-tailed deer	Not available	(Miller and Walter, 2020)
G59S Q226Q[#]	Red deer	AAU93883	(Peletto et al., 2009)
G65E Q226Q[#]	Mule deer	AY360091	(Heaton et al., 2003)
4 OR Q226Q[#]	Water deer	QAU19536	(Robinson et al., 2019)
Q95H Q226Q[+]	White-tailed deer	AY275711	(Johnson et al., 2003)
G96D Q226Q[+]	Water deer	Not available	(Roh et al., 2020)
G96R Q226Q[+]	White-tailed deer	MN577936	(Ishida et al., 2020)
G96S Q226Q[+]	White-tailed deer	AF156184	(Raymond et al., 2000)
Q95H G96S Q226Q[+]	White-tailed deer	AXH06163	(Johnson et al., 2011)
T98A Q226Q[+]	Red deer	AAU93885	(Peletto et al., 2009)
T98S Q226Q[+]	Reeves' muntjac	AGU92564	(Nalls et al., 2013)
T98S Q226E[#]	Indian muntjac	PRJNA479821	(Farre et al., 2019)
S100N Q226Q[+]	White-tailed deer	MG856917	(Brandt et al., 2015)
G96S S100N Q226Q[+]	White-tailed deer	AXH06168	(Brandt et al., 2015)
S100G Q226E[+]	Sika deer	EF057409	(Jeong et al., 2007)
N103I Q226Q[+]	White-tailed deer	MG856925	(Brandt et al., 2015)
N103T Q226Q[+]	White-tailed deer	QKI86945	(Zink et al., 2020)
K109Q Q226Q[+]	Moose	JQ290077	(Wik et al., 2012)
A116G Q226Q[+]	Mule deer	AAP33275	(Heaton et al., 2003)
A123T Q226Q[+]	White-tailed deer	MG856916	(Brandt et al., 2015)
G96S A123T Q226Q[+]	White-tailed deer	AXH06166	(Brandt et al., 2015)
G129S Q226Q[+]	Reindeer	DQ154294	(Happ et al., 2007)
M132L Q226E[+]	Elk	AF016228	(O'Rourke et al., 1998)
S138N Q226Q[+]	Reindeer	DQ154292	(Happ et al., 2007)
S138N Q226E[+]	Fallow deer	AY286007	(Rhyan et al., 2011)
N103T R151H Q226Q[+]	White-tailed deer	QMT15740[+]	(Zink et al., 2020)
Y153F Q226Q[+]	Reindeer	MT361766	(Arifin et al., 2020)
T98A P168S Q226Q[+]	Red deer	ABS87880	(Peletto et al., 2009)
V2M G129S V169M Q226Q*	Reindeer	DQ154295	(Happ et al., 2007)
D170G Q226Q[+]	Water deer	Not available	(Roh et al., 2020)
N176D Q226Q[+]	Reindeer	JQ290075	(Wik et al., 2012)
G96C A123T N176D Q226Q[#]	Reindeer	EU032303	(Perucchini et al., 2008)
V187I Q226Q[+]	Black-tailed deer	QMT15661[+]	(Zink et al., 2020)
K25R T191A Q226E*	Elk	ABS87885	(Perucchini et al., 2008)
G96S V192I Q226Q[+]	Florida Key deer	MT944346	(Perrin-Stowe et al., 2020)
G96S K197E Q226Q[+]	White-tailed deer	MZ913400	(Ott-Conn et al., 2021)
K207M Q226Q[+]	Reindeer	MW557844	(Güere et al., 2022)
M208I Q226E[+]	Red deer	UFX77122	(Kaluz et al., 1997)
T98S N173S T177N M208I Q226Q[+]	White-tailed deer	QMT15320[+]	(Zink et al., 2020)
T98S A136V Q171R N173S T177N M208I Q226Q[+]	White-tailed deer	QMT15321[+]	(Zink et al., 2020)
M209I Q226Q[+]	Moose	DQ154298	(Huson and Happ, 2006)
T36N M209I Q226Q[#]	Moose	Not available	(Wik et al., 2012)
S100R M209I Q226Q[+]	Moose	QHZ32187	(Cullingham et al., 2020)
R211Q Q226Q[+]	Reindeer	MW557845	(Güere et al., 2022)
Q215K Q226Q[+]	White-tailed deer	MZ913401	(Ott-Conn et al., 2021)
S225C Q226Q[#]	White-tailed deer	QKI86681	(Zink et al., 2020)
S225F Q226Q[+]	Mule deer	QKI86681	(Brayton et al., 2004)
S225Y Q226Q[+]	Reindeer	JQ290076	(Wik et al., 2012)
Q226Q[+]	Mule deer	AY330343	(Cervenakova et al., 1997)
Q226E[+]	Elk	AF156183	(Cervenakova et al., 1997)
Q226K[+]	White-tailed deer	MN390181	(Vázquez-Miranda and Zink, 2020)
Q226R[+]	White-tailed deer	Not available	(Wilson et al., 2009)
Q226Q Q230L[+]	White-tailed deer	Not available	(Wilson et al., 2009)
Q226Q P242L[#]	Reindeer	MT361767	(Arifin et al., 2020)
Q226Q I247L[#]	Red deer	QAU19537	(Robinson et al., 2019)
Q226E F249V[#]	Axis deer	MT996497	(Buchholz et al., 2021)
G7C S225F Q226Q L253F[#]	Mule deer	QMT15197[+]	(Zink et al., 2020)

Variants marked with [#] were excluded from the present study because a) their amino acid substitutions, compared to the reference sequence (Q226Q), are not located in the PK-resistant core of PrP^{Sc}, or b) one of their polymorphisms introduces an extra cysteine, increasing the propensity for aggregation during folding into the native state.
Variants marked with * were included in this study, excluding amino acid changes outside the PK-resistant core of PrP^{Sc}.
Accession numbers marked with [+] contain errors in their GenBank files: the corresponding author of the original publication, kindly provided the raw data, allowing us to determine the correct sequences, as indicated in this study.

3.2. Variants of cervid rec-PrP exhibit similar thermostability

To compare the thermostability of distinct cervid PrP variants, the melting temperature (T_m) of all 45 recombinant proteins was analyzed using circular dichroism (CD). As depicted in Fig. 1 and Table 2, the T_m values of the variants were similar, ranging between 67 and 70 °C in most cases, with a mean of 68.5 °C and a standard deviation of 1.7. The T_m of the reference cervid sequence, Q226Q, is 67.7 °C. The highest T_m observed was 72.4 °C for the variant T98S A136V Q171R N173S T177N M208I Q226Q, while the lowest was 65.7 °C for the variant T98A P168S Q226Q.

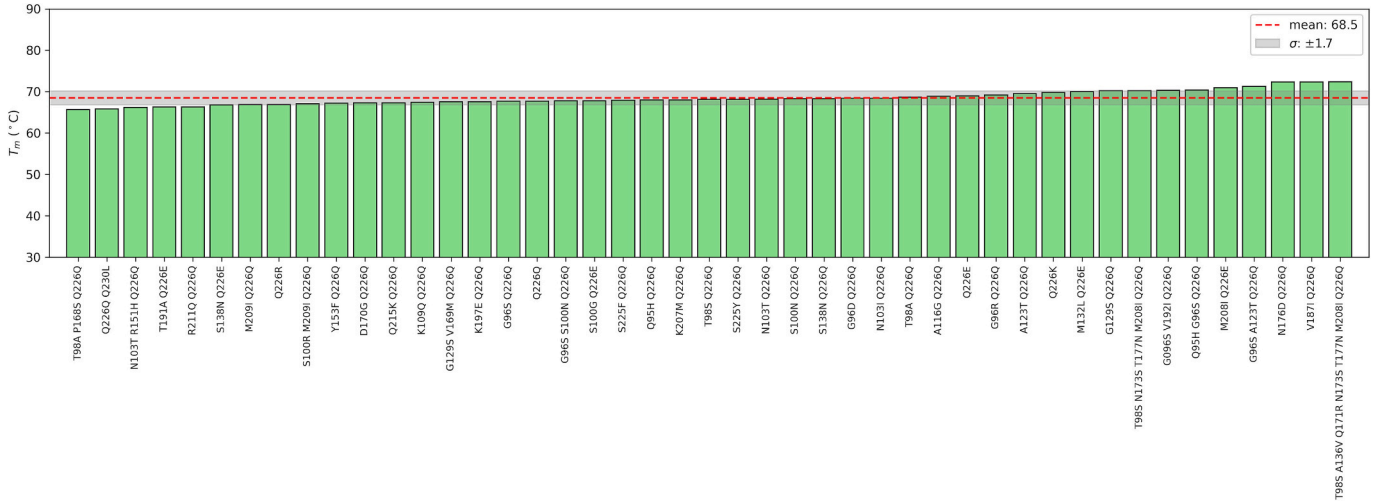

Fig. 1. Experimental determination of T_m for cervid PrP variants. Melting temperatures (T_m) of 45 cervid PrP variants was measured by circular dichroism (CD). With a mean T_m of 68.5 and a standard deviation of ±1.7, the T_m values for most variants range from 67 to 70 °C. The variants are ordered from the one with the lowest T_m, the T98A P168S Q226Q variant (65.7 °C), to the one with the highest T_m, the T98S A136V Q171R N173S T177N M208I Q226Q variant (72.4 °C), with the reference sequence Q226Q showing a T_m of 67.7 °C.

3.3. Molecular dynamics simulations of the variants of cervid PrP

We ran microsecond, all-atom molecular dynamics (MD) simulations to explore the impact of amino acid substitutions on the structure and flexibility of the crystallographically resolved PrP^C from mule deer, and therefore, results must be interpreted within this amino acid context. To this end, we considered only those cervid variants in which polymorphisms are located in the 132–229 segment (26 variants, [Table 2]), extending from strand β1 to the end of helix α3 (Fig. 2A). Such amino acid changes are broadly distributed over the PrP^C structure, with highest frequency on helices α2 and α3 (Fig. 2A).

For each variant, we ran ten independent AlphaFold 2 structure predictions and used the highest confidence one (Fig. 2B) as the initial geometry for classical MD simulations. The predicted Local Distance Difference Test (pLDDT) scores of the structures are shown in Table 2 and indicate that all variants are predicted with high confidence (pLDDT scores >91). Additionally, we computed the α-carbon RMSD of the predictions with respect to a high-resolution crystallographic structure of the deer prion protein (PDB 4YXH); all structures show low deviations (below 1.5 Å, Table 2), indicating a high structural similarity to the crystallographic reference and validating the use of AlphaFold structures to initialize MD simulations.

For each variant, we ran a single 1 μs simulation and monitored the evolution of backbone root mean square deviation (RMSD), secondary structure content, and per-residue root mean square fluctuations (RMSFs). Backbone RMSD remains below 4 Å throughout the whole simulation for all variants, demonstrating that mutations do not significantly affect the PrP^C structure (Supplementary Fig. 1). Per-residue RMSF values show that the most flexible region of the models is the C-terminus (Supplementary Fig. 2). Some modest flexibility is also observed at the tip of helix α2 and at the loop connecting helix α2 with helix α3 (RMSFs up to 6 Å). RMSF differences observed between variants are small and distributed over the whole protein, falling within the expected range of simulation variability. These differences cannot be specifically attributed to the amino acid mutations but rather reflect the stochastic nature of the randomized velocities used to initialize the MD simulations. Finally, analysis of the secondary structure content along the MD simulations shows a high degree of conservation of the secondary structure elements present in the initial models, showing only small fluctuations in the α-helix content corresponding to partial and reversible unwinding of α-helix tips (Supplementary Fig. 3). These results agree with the thermodynamic signatures measured by CD for cervid PrP variants, indicating that the introduced mutations had minimal effects on the globular domain's structure and dynamics under the simulation conditions tested. Such an outcome is expected, since more disruptive mutations would compromise the protein's native conformation, thereby hindering its function and perturbing cellular homeostasis.

3.4. Cervid rec-PrP variants show diverse spontaneous misfolding propensities, with key polymorphisms conferring resistance

After dialyzing the proteins and ensuring proper concentrations, each substrate underwent a PMSA procedure designed to induce spontaneous misfolding of rec-PrP into *bona fide* prions. This method, initially developed with bank vole and mouse rec-PrP (Eraña et al., 2023; Pérez-Castro et al., 2025), was later modified to establish a ranking of spontaneous misfolding propensity among diverse rec-PrP variants from numerous mammals (Erana et al., 2024). The resulting approach involved four consecutive 24-h PMSA rounds, each with 8 replicates per substrate, where half of the replicates were supplemented with 1 mm diameter glass beads and the other half were supplemented with 0.1 mm diameter glass beads.

To quantify the propensity for spontaneous misfolding in each analyzed PrP, a formula was developed considering the number of positive replicates for protease-resistant misfolded rec-PrP ($rec\text{-}PrP^{res}$) in each round and under varying conditions. According to this formula, a protein showing 100 % positive replicates for $rec\text{-}PrP^{res}$ in the first PMSA round received a score of 100 %. In contrast, a protein for which $rec\text{-}PrP^{res}$ was undetected in any replicate or PMSA round received a score of 0 %. Intermediate scores were determined based on the number of positive replicate tubes in each round and under varying conditions.

(https://www.prpdex.com/PrPs/instructions/scores.pdf).

Applying this methodology to the 45 PrP variants analyzed in the present study, the spontaneous misfolding proneness of each variant was quantified (Fig. 3, Table 2). Remarkably, 67 % of these variants exhibited high spontaneous misfolding proneness, with scores of 75 % or higher. Notably, the two most frequent variants, Q226Q and Q226E, fell into this high misfolding proneness group. On the other hand, among the remaining 33 % of variants with lower spontaneous misfolding proneness, many featured polymorphisms in the β2-α2 loop or at the end of the third α-helix of the PrP.

Looking at the single-mutant variants, 5 mutations clearly emerge as protective towards misfolding: Q215K, with a score of 36 % (36 %),

Table 2
Polymorphic cervid PrP variants: PrP^C model (residues 132–229) used for molecular dynamics (MD) simulations, predicted Local Distance Difference Test (pLDDT) score of the highest-confidence AlphaFold model used as the starting geometry for MD, α-carbon root-mean-square deviation (RMSD) with respect to the crystallographic structure of deer PrP^C (PDB ID: 4YXH), RMSD with respect to the model backbone, α-helix content (%), experimental melting temperature (°C), and spontaneous misfolding score (%).

Polymorphic variant	PrP^C model (132–229)	pLDDT score	RMSD w.r.t. PDB 4YXH (Å)	RMSD backbone (Å) (mean ± SD)	α-helix content (%) (mean ± SD)	T_m (°C)	Score (%)
Q95H Q226Q	NA	NA	NA	NA	NA	68.0	83.93
G96D Q226Q	NA	NA	NA	NA	NA	68.4	100.00
G96R Q226Q	NA	NA	NA	NA	NA	69.2	89.29
G96S Q226Q	NA	NA	NA	NA	NA	67.7	96.43
Q95H G96S Q226Q	NA	NA	NA	NA	NA	70.4	79.29
T98A Q226Q	NA	NA	NA	NA	NA	68.7	96.43
T98S Q226Q	NA	NA	NA	NA	NA	68.1	96.43
S100N Q226Q	NA	NA	NA	NA	NA	68.3	91.07
G96S S100N Q226Q	NA	NA	NA	NA	NA	67.8	82.14
S100G Q226E	NA	NA	NA	NA	NA	67.8	96.43
N103I Q226Q	NA	NA	NA	NA	NA	68.4	82.14
N103T Q226Q	NA	NA	NA	NA	NA	68.2	96.43
K109Q Q226Q	NA	NA	NA	NA	NA	67.4	100.00
A116G Q226Q	NA	NA	NA	NA	NA	68.9	100.00
A123T Q226Q	NA	NA	NA	NA	NA	69.5	87.50
G96S A123T Q226Q	NA	NA	NA	NA	NA	71.3	39.29
G129S Q226Q	NA	NA	NA	NA	NA	70.2	83.57
M132L Q226E	M132L Q226E	93.26	1.20	1.81 ± 0.33	55.95 ± 1.76	70.0	89.29
S138N Q226Q	S138N	93.56	1.13	1.79 ± 0.39	56.47 ± 1.78	68.3	89.29
S138N Q226E	S138N Q226E	93.46	1.22	1.69 ± 0.30	55.92 ± 1.89	66.8	100.00
N103T R151H Q226Q	R151H	92.39	1.14	1.64 ± 0.41	57.40 ± 1.84	66.2	72.50
Y153F Q226Q	Y153F	92.72	1.04	2.33 ± 0.68	53.98 ± 2.46	67.2	67.86
T98A P168S Q226Q	P168S	92.83	1.15	2.37 ± 0.53	53.29 ± 1.74	65.7	43.57
G129S V169M Q226Q	V169M	92.75	1.14	1.87 ± 0.29	55.64 ± 2.25	67.6	21.43
D170G Q226Q	D170	92.17	1.16	2.12 ± 0.41	54.83 ± 2.76	67.3	36.61
N176D Q226Q	N176D	92.59	1.14	1.52 ± 0.33	57.22 ± 2.26	72.3	100.00
V187I Q226Q	V187I	92.43	1.17	2.17 ± 0.53	55.64 ± 1.85	72.3	100.00
T191A Q226E	T191A Q226E	92.49	1.15	1.92 ± 0.30	52.93 ± 1.86	66.3	100.00
G96S V192I Q226Q	V192I	92.49	1.20	1.93 ± 0.39	53.92 ± 2.20	70.3	92.86
K197E Q226Q	K197E	92.78	1.27	2.25 ± 0.28	55.12 ± 1.85	67.6	100.00
K207M Q226Q	K207M	94.09	1.25	1.72 ± 0.35	55.47 ± 2.39	68.0	89.29
M208I Q226E	M208I Q226E	93.12	1.23	1.76 ± 0.32	56.84 ± 1.08	70.9	48.21
T98S N173S T177N M208I Q226Q	N173S T177N M208I	93.13	1.21	1.71 ± 0.37	56.72 ± 1.87	70.2	54.29
T98S A136V Q171R N173S T177N M208I Q226Q	A136V Q171R N173S T177N M208I	94.17	1.20	1.69 ± 0.47	56.37 ± 2.56	72.4	0.00
M209I Q226Q	M209I	92.30	1.46	1.90 ± 0.29	55.71 ± 1.77	66.9	75.00
S100R M209I Q226Q	M209I	92.30	1.46	1.90 ± 0.29	55.71 ± 1.77	67.1	45.71
R211Q Q226Q	R211Q	91.35	0.72	2.34 ± 0.62	56.80 ± 1.97	66.3	91.07
Q215K Q226Q	Q215K	92.81	1.27	1.80 ± 0.44	56.53 ± 1.67	67.3	35.71
S225F Q226Q	S225F	92.13	1.19	1.76 ± 0.34	55.46 ± 2.63	67.9	52.86
S225Y Q226Q	S225Y	92.51	1.26	1.38 ± 0.20	57.04 ± 1.77	68.1	48.93
Q226Q	Q226Q	92.09	1.17	1.73 ± 0.44	57.70 ± 1.52	67.7	100.00
Q226E	Q226E	92.74	1.15	1.53 ± 0.28	57.38 ± 1.23	69.0	100.00
Q226K	Q226K	92.20	1.24	1.71 ± 0.23	53.72 ± 2.09	69.8	75.00
Q226R	Q226R	92.15	1.26	1.94 ± 0.49	55.51 ± 1.80	66.9	65.00
Q226Q Q230L	NA	NA	NA	NA	NA	65.8	50.00

NA (Not Available) marks those variants with polymorphisms exclusively in the N-terminal region (amino acids 23–131 and 230–234), excluded from the *in silico* analysis. The high pLDDT scores indicate that all variants were predicted with high confidence. The low RMSD with respect to the structure of the deer prion protein (PDB 4YXH) denote a high structural similarity to the crystallographic reference. Larger backbone RMSD values and greater fluctuations in α-helix content reflect increased flexibility.

† The melting temperature (T_m) was determined using circular dichroism (CD).

‡ The spontaneous misfolding score was calculated based on the results from serial PMSA rounds without the addition of a preformed seed (number of replicates showing rec-PrP^{res} and PMSA round in which they were first detected). A higher score correlates with a greater propensity to misfold, while a lower score implies reduced misfolding proneness, with 0 indicating resistance to spontaneous misfolding.

D170G (37 %), S225Y/F (49 %/53 %), Q230L (50 %). Other mutations with moderate or even low protective effect such as M209I (75 %), G129S (84 %), A123T (88 %) or G96S (96 %), appear also in quite resistant double-mutants thus revealing epistatic effects: G129S V169M (21 %), G96S A123T (39 %), S100R M209I (46 %). Finally, mutations such as V169M, P168S and M208I do not appear alone but also seem to have a significant protective effect when combined in double mutants: G129S V169M (21 %), T98A P168S (44 %), M208I Q226E (48 %).

Among all the tested proteins, only one variant, T98S A136V Q171R N173S T177N M208I Q226Q, was unable to spontaneously misfold even after four serial rounds of PMSA (0 %). To identify the specific amino acid substitutions responsible for this resistance, we produced new rec-PrP, each one featuring only one of the polymorphisms present in the T98S A136V Q171R N173S T177N M208I Q226Q variant. Following the described protocol, these new variants underwent the same methodology, and their spontaneous misfolding proneness was quantified (Supplementary Fig. 4). The low scores of four of them confirmed the influence on the spontaneous misfolding process of amino acids located in both the β2-α2 loop (Q171R, 7 %, and N173S, 9 %) and at the end of the third α-helix of the PrP (M208I, 25 %), with also a notable effect of mutation A136V (28 %).

Overall, clear polymorphic hotspots appear to be involved in resistance to misfolding: amino acids 168–173, 208–209, 215 and 225–226.

All detailed information for each variant analyzed in this study is

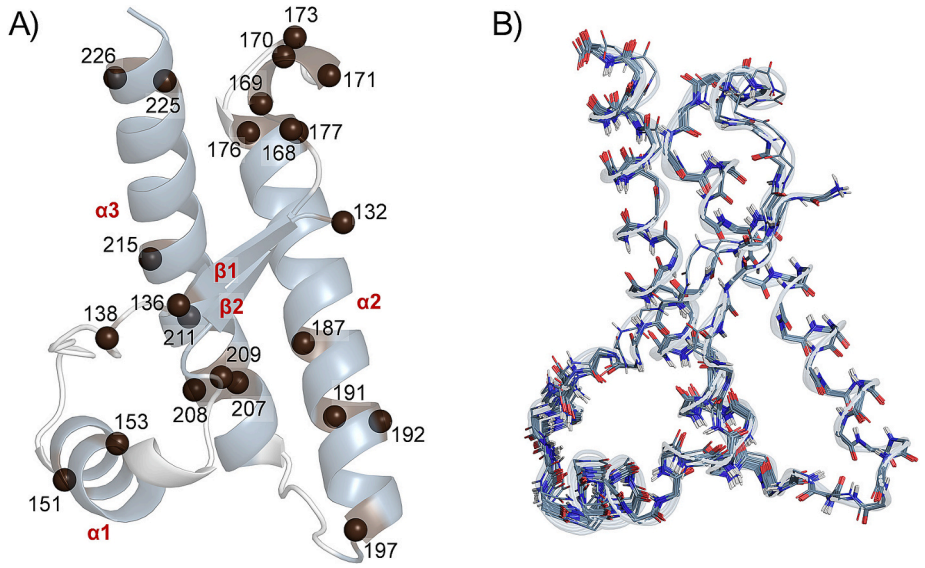

Fig. 2. AlphaFold structure of cervid PrP^{C} variants. A) Cartoon representation of an AlphaFold 2 structure of the reference variant Q226Q. Amino acid positions undergoing mutation are shown as brown spheres. Secondary structure elements of the PrP^{C} structure are labelled in red (β1: residues 132–136; α1: 148–156; β2: 162–166; α2: 176–198; α3: 204–230). B) Overlay of the AlphaFold 2 models of the 26 variants considered in this work. Only backbone atoms are shown for clarity. (For interpretation of the references to colour in this figure legend, the reader is referred to the web version of this article.)

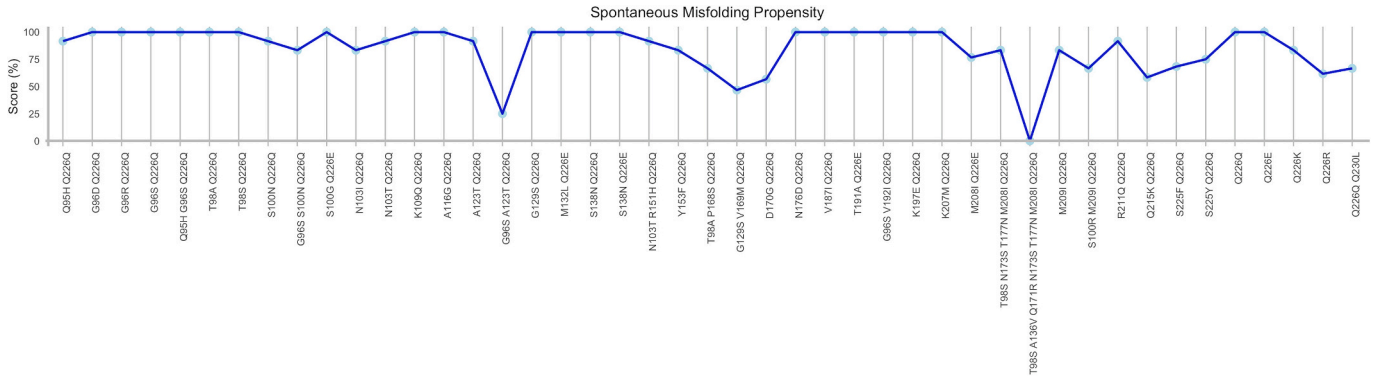

Fig. 3. Spontaneous misfolding propensity of the cervid PrP variants. The propensity of each cervid PrP variant to misfold spontaneously was assessed through four serial rounds of PMSA. Each PMSA round consisted of 8 replicates, with the PMSA substrate containing conversion buffer, recombinant PrP (rec-PrP), and dextran sulfate. Half of the samples contained 0.1 g of 1 mm glass beads, and the other half 0.1 g of 0.1 mm glass beads. After each round, the products were diluted 1:10 into fresh PMSA substrate, and the next round was initiated. At the end of each 24-h round, products were analyzed for the presence of PrP^{res} by proteinase K (PK) digestion, electrophoresis, and total protein staining. Based on the results, each variant was assigned a score (ranging from 0 to 100) that reflects its propensity to spontaneously misfold. A higher score represents a greater propensity for misfolding, while a score of 0 suggests resistance to misfolding. From the 45 PrP variants analyzed, 67 % show high misfolding proneness with scores over 75, including the reference sequences Q226 and Q226E, while the other 33 % showed low misfolding scores, with variant T98S A136V Q171R N173S T177N M208I Q226Q being the only one completely unable to misfold. The misfolding score (%) is shown on the y-axis, with each cervid PrP variant displayed on the x-axis.

compiled in PrPdex files (Supplementary Fig. 5), which can also be accessed at https://prpdex.com/cervidae/.

3.5. *Spontaneously misfolded cervid PrP are bona fide infectious prions*

While our prior research utilizing PMSA to induce spontaneous misfolding in rec-PrP already demonstrated the efficacy of this methodology in generating *bona fide* prions (Erana et al., 2024), the biological significance of the present study was further validated through the characterization of one of the rec-PrP^{res} *via* electron microscopy and bioassay. For this purpose, an ensemble of conformers resulting from the spontaneous misfolding of one replicate of the cervid reference amino acid sequence (Q226Q) rec-PrP was chosen.

The selected ensemble of conformers, named Deer-Dx-D, was partially digested with PK and purified through density gradient and ultracentrifugation. This procedure allowed for the distinction of a halo, which was collected and processed for visualization using transmission electron microscopy (TEM). As depicted in Supplementary Fig. 6, Deer-Dx-D forms fibrillar structures that assemble with one another. The resulting architecture is very similar to the prion rods observed in PrP^{Sc} samples purified from the brains of diseased animals (Terry et al., 2019).

After confirming the ultrastructural resemblance of these recombinant cervid prions to brain-derived mammalian prions, Deer-Dx-D was used to perform intracerebral inoculations into TgVole 1× mice (Fernández-Borges et al., 2017). These transgenic mice express the PrP^{C} of the bank vole, a species considered the universal acceptor of prions due to its high susceptibility to TSE. Through this bioassay, Deer-Dx-D was confirmed as a *bona fide* prion capable of inducing prion disease in a susceptible animal model after 342 ± 33 days post-inoculation (dpi) (see Supplementary Fig. 7). Following this incubation period, the

inoculated mice exhibited clinical signs such as weight loss, kyphosis, and incoordination, among others. Additionally, a three-banded PrP^{res} signal was observed after proteinase K (PK) digestion and western blotting (WB) of their brains (Fig. 4). Neuropathological characterization of these brains revealed the hallmarks of prion diseases, including spongiosis, prion protein deposits and gliosis. The two most affected brain areas, the striatum and thalamus, of one representative diseased mouse, compared to one non-infected TgVole 1× as a negative control, are shown in Fig. 5.

Biochemical analyses revealed the presence of at least two different phenotypes among the challenged animals. PK digestion and WB of the brains from inoculated mice exposed two distinct electrophoretic patterns: one exhibiting a higher molecular weight and another showing a lower molecular weight (Fig. 4B). Furthermore, while intense gliosis was present in all analyzed animals, neuropathological characterization of these brains unveiled variations in the severity and distribution of vacuolation and the quantity of PrP^{res} deposits among individuals (Fig. 4A). However, no clear correlation could be established between the different WB patterns and the distribution of vacuolation, amount of PrP^{res} deposits, nor the incubation time.

For the second passage, we selected the brain of a mouse that presented an incubation period of 336 dpi, which was closest to the mean of the whole group (342 ± 33). Biochemical characterization of this brain revealed a low molecular weight electrophoretic pattern of PrP^{Sc} (Fig. 4B and D). Neuropathological analysis of the brain of this mouse showed considerable vacuolation in the striatum, thalamus, midbrain and medulla oblongata, accompanied by substantial PrP^{res} deposits in the striatum, thalamus, midbrain, medulla oblongata and in the hippocampus (Fig. 4A).

This second passage significantly reduced the incubation period from inoculation to terminal disease to 91 ± 3 dpi (Supplementary Fig. 7). The inoculated animals exhibited clinical signs similar to those observed in the first passage. Consistent with the previous passage findings, western blotting of the brains from inoculated animals after proteinase K digestion revealed three-banded PrP^{res} signals (Fig. 4D). Neuropathological characterization demonstrated a lesion profile resembling that observed in the first passage (Fig. 4C). Supplementary Fig. 8 illustrates the striatum and thalamus of infected TgVole 1× mice, where spongiosis, PrP^{res} deposits, and gliosis were most pronounced in comparison with a non-infected negative control.

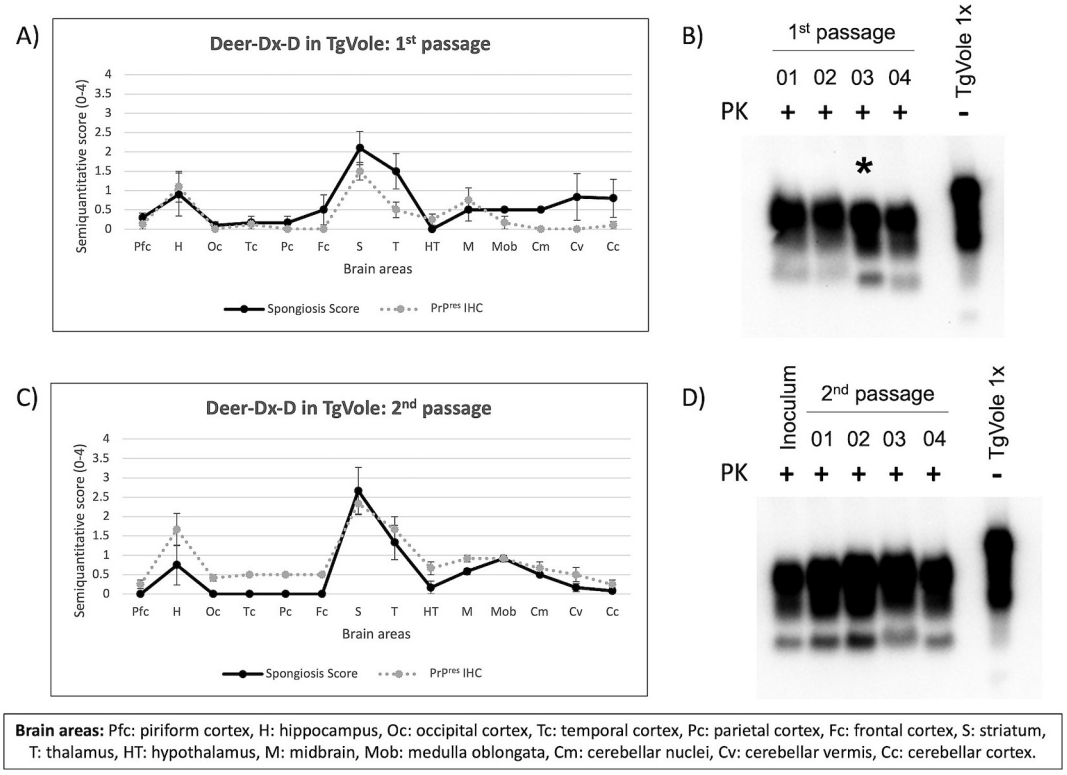

Brain areas: Pfc: piriform cortex, H: hippocampus, Oc: occipital cortex, Tc: temporal cortex, Pc: parietal cortex, Fc: frontal cortex, S: striatum, T: thalamus, HT: hypothalamus, M: midbrain, Mob: medulla oblongata, Cm: cerebellar nuclei, Cv: cerebellar vermis, Cc: cerebellar cortex.

Fig. 4. *In vivo* characterization of the spontaneously misfolded ensemble of conformers Deer-Dx-D inoculated in TgVole 1×, transgenic mouse line expressing bank vole PrPC. A) Spongiform lesion profile and PrP^{res} deposition patterns in the brains of TgVole 1× mice inoculated with Deer-Dx-D at first passage. A semi-quantitative score (0–4) shown on the y-axis is used to assess spongiform lesion severity (black dots and line) and PrP^{res} deposit levels (gray dots and dotted gray line) in 14 different regions of the central nervous system of these mice, described along the x-axis. The regions most affected by spongiosis include the hippocampus, striatum, thalamus, midbrain, medulla oblongata, cerebellar nuclei, cerebellar vermis, and cerebellar cortex. PrP^{res} deposits colocalized with spongiform lesions in most regions, particularly in the hippocampus, striatum, thalamus, and midbrain. B) Biochemical analysis of the PrP^{Sc} from TgVole 1× brains inoculated with Deer-Dx-D at first passage by Western blot. Four representative samples (01–04) from the TgVole 1× animals inoculated with Deer-Dx-D PMSA product are presented post-PK digestion (+), along with an uninfected and undigested (−) TgVole 1× control, using the BAR224 antibody (epitope at residues 144–154, dilution 1:1000). The presence of at least two distinct electrophoretic patterns suggests that the Deer-Dx-D might consist of multiple substrains. The brain homogenate used as inoculum for the second passage is marked with an asterisk (*). C) Spongiform lesion profile and PrP^{res} deposition patterns in the brains of TgVole 1× mice inoculated with Deer-Dx-D at second passage. The y-axis represents the semi-quantitative score (0–4), and the x-axis covers different CNS regions. Spongiosis (black dots and line) and PrP^{res} deposition (gray dots and dotted gray line) were more pronounced in the hippocampus, striatum, and thalamus after the second passage. Notably, PrP^{res} deposits were more widely distributed throughout the CNS following this passage. D) Biochemical analysis of the PrP^{Sc} from TgVole 1× inoculated with Deer-Dx-D after the second passage. The brain homogenate from the diseased TgVole 1× selected as the inoculum for the second passage, along with four representative samples (01–04), were analyzed after PK digestion (+), as well as one uninfected TgVole 1× control (−), using the BAR224 antibody. Similar to the first passage, at least two distinct electrophoretic patterns were visible, further suggesting that the inoculum might consist of a mixture of substrains, even after two passages. MW: Molecular weight marker; PK: Proteinase K; IHC: Immunohistochemistry performed with 6C2 antibody (epitope at residues 111–118, dilution 1:1000).

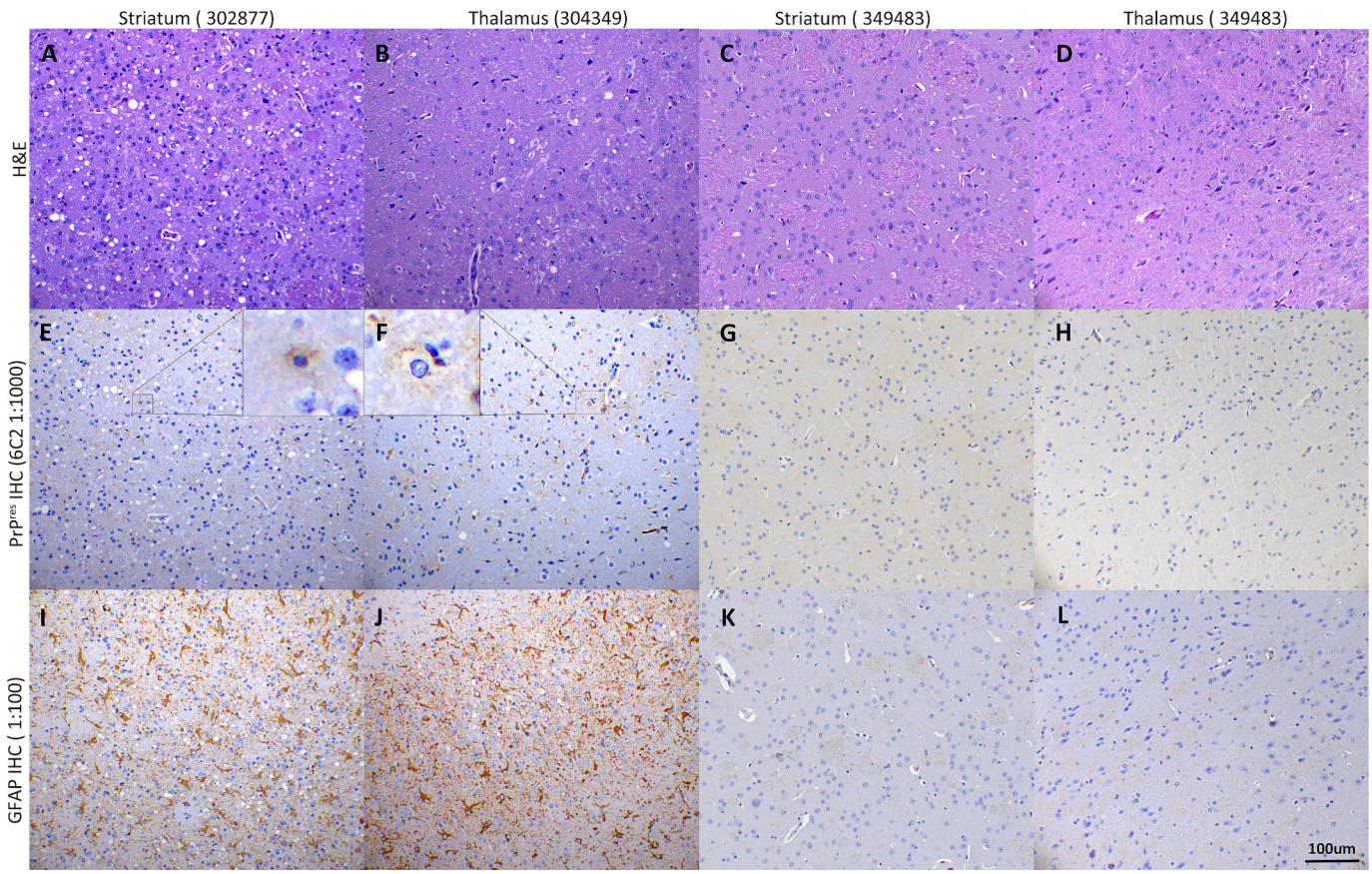

Fig. 5. Neuropathological characterization of TgVole 1× mouse brains inoculated with the ensemble of conformers Deer-Dx-D. Images display the two most affected brain regions, the striatum and thalamus, from two representative diseased mice (302,877 and 304,349) inoculated with Deer-Dx-D PMSA product (first passage), alongside a non-infected TgVole 1× (349483) as a negative control. Hematoxylin and eosin staining (H&E) showed severe spongiosis in the striatum of the diseased animals (A) and milder spongiosis in the thalamus of these mice (B), while no spongiosis was found in the brain regions of the non-infected controls (C, D). Immunohistochemistry for PK-resistant prion protein (PrP^{res} IHC) using monoclonal antibody 6C2 (epitope at residues 111–118, dilution 1:1000) revealed a fine granular immunostaining pattern in the striatum of the infected mice, often associated with glial cells (E), and a synaptic-like punctate pattern in the thalamus, observed both intraneuronally and perineuronally (F). No PrP^{res} deposits were observed in the negative controls (G, H). Glial fibrillary acidic protein immunohistochemistry (GFAP IHC) detected intense astrogliosis, with hyperplasia and hypertrophy of astrocytes in both the striatum (I) and thalamus (J), as well as in all regions showing spongiform changes; the corresponding brain areas in the uninfected controls lacked these features (*K*,*L*). All images were taken at the same magnification (20× objective), bar: 100 μm.

Interestingly, despite observing no significant differences in the incubation period among the challenged animals, biochemical analysis of the second passage mice brains again revealed two distinct electrophoretic patterns (Fig. 4D). These patterns mirrored those found in the first passage; one characterized by a lower molecular weight, identical to the pattern of the selected inoculum, and the other by a higher molecular weight. Neuropathological examination revealed that all animals presented punctate PrP^{res} deposits, both intraneuronal and within the neuropil of the brainstem. In the striatum, PrP^{res} deposits appeared as bigger aggregates, accompanied by intense vacuolation and astrogliosis. While these were the most common features observed in this group of six mice, additional variations were noted: two animals exhibited severe spongiosis, and marked gliosis in the hippocampus with incipient PrP^{res} plaques in the albeus, along with fine punctate labelling in the stratum oriens (Supplementary Fig. 9 A, D, and G); two other animals showed conspicuous plaques in the hippocampus albeus but with milder to absent spongiosis and the astrogliosis restricted only to the vicinity of the plaques (Supplementary Fig. 9 B, E, and H), and the remaining two animals were characterized by the absence of PrP^{res} specific immunolabeling patterns in the hippocampus and a mild to absent astrogliosis, lacking spongiform lesions in that region (Supplementary Fig. 9C, F, and I). One of the mice presenting hippocampal plaques also displayed the higher molecular weight electrophoretic pattern when its brain was analyzed through proteinase K digestion and western blot. Conversely, the other mouse with hippocampal plaques showed the lower molecular weight electrophoretic pattern. Collectively, these findings suggest the presence of at least three different phenotypes following the second passage, highlighting the complexity and diversity generated by an *in vitro* system through the promotion of spontaneous misfolding, likely mirroring processes that occur in a more biological context.

4. Discussion

We conducted a comprehensive characterization of different variants of cervid PrP, assessing the effect of various polymorphisms on flexibility, structure, stability, and spontaneous misfolding proneness.

The high prevalence of CWD in North America (Moreno and Telling, 2018), and the cases described in Nordic European countries (Benestad et al., 2016; Pirisinu et al., 2018; Vikoren et al., 2019) have raised alarms about the emergence of new strains and their zoonotic potential (Tranulis, 2021). The well-established relationship between amino acid changes and perturbations in the interspecies barrier (Angers et al., 2014; Bett et al., 2012; Scott et al., 1993) has prompted several studies focused on genotyping different cervid populations and characterizing their *PRNP* gene (Arifin et al., 2021), leading to the description of up to 59 variants. Within the PK-resistant core of the PrP^{Sc} (residues 92–230),

42 different polymorphisms were identified in cervid PrP. Building on previous work from our laboratory, we compared all the polymorphic variants from cervid PrP to the sequences of every wild-type mammal PrP described to date, which are publicly available on the PrPdex website (https://prpdex.com/) (Erana et al., 2024). Thus, we identified 14 unique polymorphisms in the cervid PrPs within residues 100–230 (bank vole numbering), the region covered by PrPdex. These polymorphisms—N103I, N103T, K109Q, A116G, A123T, R151H, Y153F, P168S, T191A, K197E, K207M, R211Q, Q215K, and Q226K—had not been reported in other wild-type mammals, rendering their effects on protein flexibility, stability, or misfolding susceptibility unknown. While no relation between the polymorphism and the disease has been reported, our results show a 100 % spontaneous misfolding propensity score, suggesting that a potential link cannot be discarded. This is exemplified by the change A116G in white-tailed deer PrP, which modifies NA CWD properties, giving rise to the strain 116 AG (Hannaoui et al., 2021). Additionally, the variant K109Q present in moose PrP has been found in some animals affected by Nordic CWD (Sola et al., 2023).

Apart from these cervid-exclusive polymorphisms, other amino acid changes within cervid sequences have been previously linked to misfolding susceptibility or strain emergence. For instance, M132L is a polymorphism described in elk PrP (Schatzl et al., 1997) that is related to a low susceptibility to NA CWD (Green et al., 2008) and is able to modify the original strain, resulting in the CWD strain LL132 (Moore et al., 2020). While most wild-type mammal PrPs have M at position 132, the presence of L could only be found in 1.8 % of the species whose PrP has been sequenced, all of them characterized by low spontaneous misfolding scores according to PrPdex (https://prpdex.com/) (Erana et al., 2024). However, while the misfolding score of the M132L Q226E variant is lower than that of the cervid reference variant, it still shows a high score. This suggests that, while the variant may be resistant to the NA CWD strain, its high potential for spontaneous misfolding could lead to the emergence of new strains, potentially resembling the LL132 strain or even entirely new, unstable strains, as observed in some Nordic CWD cases. The position 132 of cervid PrP is equivalent to position 129 of human PrP, which is notable for the existence of a dimorphism (129 M or 129 V) that modulates the susceptibility of humans to certain prion diseases, such as Variant Creutzfeldt-Jakob disease (vCJD) (Collinge, 2001). Collectively, these facts reflect the importance of that position in terms of susceptibility. While the residue at that position of the elk variant does not match its counterpart in human PrP, there are other polymorphisms within cervid PrP that introduce amino acids present in the equivalent position of human PrP, such as N173S, T177N, and V187I. Similarly, some amino acid changes in cervid PrP match those in sheep PrP, such as T98S, N173S, T177N, and M208I, all of which are present in the same variant (Zink et al., 2020). Thus, that cervid variant shares its amino acid sequence with sheep ARQ PrP, one of the main sheep PrP genotypes along with the sheep VRQ and the sheep ARR variants (Hamir et al., 2006). Interestingly, there is another cervid variant with all those amino acid changes (T98S, N173S, T177N, and M208I) that also displays the polymorphisms A136V and Q171R (Zink et al., 2020), giving rise to a PrP that would be equivalent to a hypothetical sheep VRR PrP, which does not exist in nature. Since VRQ and ARR variants are known for their different susceptibility to scrapie (Smits et al., 1997), this could shed some light on the importance of residues 136 and 171 in terms of prion disease susceptibility. Regarding spontaneous misfolding, we have found, as expected, that Q171R variant exhibited very low susceptibility, while A136V also showed some resistance when expressed in the context of the reference cervid PrP (Supplementary Fig. 4).

Melting temperatures (T_m) are commonly used as an experimentally affordable approximation of the free energy of unfolding (ΔG_u) of proteins, which ultimately determines their thermostability (Wright et al., 2017). Changes in these properties upon mutation (ΔT_m as a proxy for $\Delta\Delta G_u$) allow inferring whether a given protein would be more or less thermostable through either kinetic or thermodynamic stabilization mechanisms (Kotov et al., 2021). In prions and related proteins with the ability to misfold into fibrillar structures, one could hypothesize that increasing the thermal resistance of the globular form of the protein to unfold might slow down misfolding by reducing the concentration of (partially) unfolded states prior to aggregation.

In our case, however, our analysis did not reveal a clear connection between melting temperatures (measured by CD) and misfolding propensities (estimated by PMSA) in the cervid PrP^C variants tested (Fig. 6A). Hence, variants with the highest measured T_m values (72 °C) showed either complete misfolding propensity (N176D Q226Q; V187I Q226Q) or no misfolding propensity (T98S A136V Q171R N173S T177N M208I Q226Q) in our hands. On the other side of the spectrum, variants with the lowest T_m values (66 °C) can preserve a full to partial misfolding propensity. Local correlations or anticorrelations within certain variants subsets are suggestive but should not be overinterpreted.

In agreement with T_m measurements, extensive MD simulations on 26 cervid PrP variants modelled based on the wild type mule deer PrP (PDB ID: 4YXH) demonstrate that they all have similar conformational and flexibility profiles in the cellular isoform, presenting essentially equivalent RMSD and per-residue RMSF profiles, with variations within the expected range of simulation variability. As expected for fully functional proteins, the secondary structure elements characteristic of the cellular isoform are likewise globally preserved, suggesting that the effect exerted by mutations on the misfolding propensity cannot be attributed to large structural or stability differences in PrP^C (Fig. 6B) but rather to the modulation of the aggregation process, or to the structure of PrP^{Sc}.

Some of the mutations described in this work have shown a certain resistance to CWD *in vivo* and, therefore, presumably to misfolding (Arifin et al., 2021). These variants include Q95H Q226Q, G96S Q226Q (Johnson et al., 2011; Robinson et al., 2012), A116G Q226Q (Hannaoui et al., 2017), M132L Q226E (Green et al., 2008), S138N Q226Q (Rhyan et al., 2011), and S225F Q226Q (Angers et al., 2014; Fox et al., 2006). Despite their reported resistance, when assessing their spontaneous misfolding propensity by PMSA, most of these showed a score higher than 80, indicating a relatively high propensity to misfold. The only exception was the S225F Q226Q variant, which displayed a score of 53, showing lower susceptibility to spontaneous misfolding.

The disparity between spontaneous misfolding in our system and *in vivo* CWD susceptibility may stem from differences in the protein's expression and the misfolding process itself. PMSA utilizes rec-PrP, while *in vivo* prion infection involves brain-derived PrP, which includes GPI anchoring and glycosylation, factors absent *in vitro*. Additionally, we study spontaneous misfolding, whereas most CWD research focuses on seed-induced propagation, where certain amino acids may play different roles. Prion propagation depends on structural compatibility between donor and acceptor PrP, while spontaneous misfolding is driven by a single PrP sequence's tendency to adopt its neurotoxic conformation. According to the quasi-species theory, when prions are transmitted to a host with a heterologous PrP, the most favored conformers in a potential mixture are selected, or the original prion strain must adapt to the new host PrP (Collinge and Clarke, 2007; Li et al., 2010). This could explain why the same polymorphic variants may exhibit distinct behaviors depending on the strain received from the donor, likely through specific interactions that are absent in spontaneous misfolding. An example of this differential behavior is seen with Nor98 compared to classical scrapie (Benestad et al., 2003; Curcio et al., 2016; Rodríguez-Martínez et al., 2010). Similarly, different Nordic moose CWD strains, hypothesized to have a spontaneous origin like Nor98 (Pirisinu et al., 2018; Tranulis, 2021), have shown different transmission properties from North American CWD when transmitted to bank voles (Nonno et al., 2020), gene-targeted (Gt) mice expressing wild-type deer or elk PrP (Bian, 2019; Bian et al., 2021; Sun et al., 2023), or Gt mice expressing cervid PrP variants (Arifin et al., 2024; Arifin et al., 2023). Therefore, our results on spontaneous misfolding propensity may not necessarily align with observations from CWD

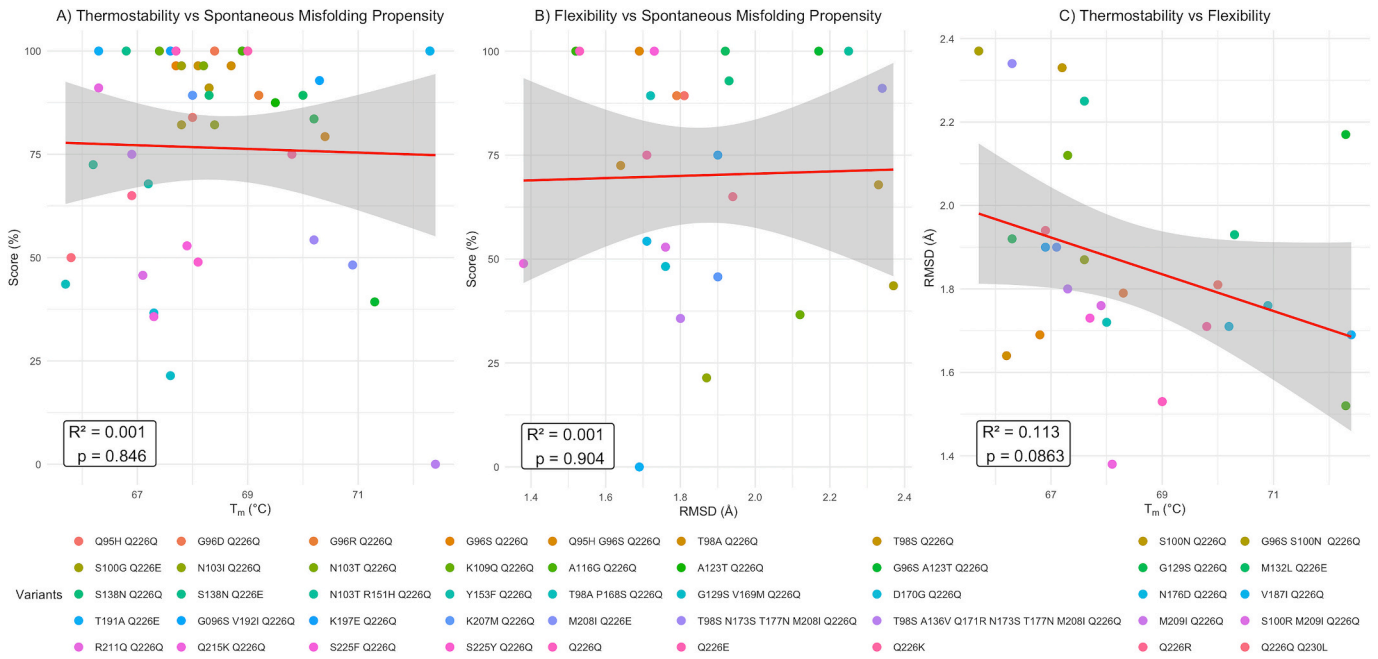

Fig. 6. Spontaneous misfolding propensity, thermostability, and protein flexibility of cervid PrP variants are not correlated. Pairwise scatter plots illustrate the relationship between the three parameters. Each variant is represented by a different colour. The calculated regression line is shown in red, with its confidence interval displayed in gray. The low slope of the regression lines and the wide confidence bands in all three plots suggest a weak or nonexistent relationship between the parameters. A) Spontaneous misfolding propensity (score, %) of cervid PrP variants, analyzed through Protein Misfolding Shaking Amplification (PMSA), plotted against thermostability, assessed as melting temperature (Tm, °C) measured by circular dichroism. No correlation is observed, as indicated by the very low coefficient of determination ($R^2 = 0.001$) and a *p*-value far above 0.05 ($p = 0.846$). B) Spontaneous misfolding propensity (score, %) plotted against protein flexibility, analyzed through molecular dynamics simulations and expressed as the root mean square deviation (RMSD, Å) of the backbone atoms (Cα, C, N) of each variant. Again, no correlation is observed ($R^2 = 0.001$; $p = 0.904$). C) Protein flexibility (RMSD, Å) plotted against thermostability (Tm, °C). The statistical parameters obtained ($R^2 = 0.113$; $p = 0.0863$) suggest a weak relationship between these parameters. However, the lack of statistical significance ($p > 0.05$) and the low explanatory power ($R^2 = 0.0863$) indicate that this correlation is likely due to random variation and can be considered negligible. (For interpretation of the references to colour in this figure legend, the reader is referred to the web version of this article.)

transmission experiments but could help identify polymorphic PrP variants or cervid species where spontaneous prion disease is more likely. This is exemplified by the fact that CWD-diseased moose found in nature so far presented the cervid PrP reference sequence (Q226Q) or the variant K109Q Q226Q, both of which displayed a score of 100 in our study.

In addition to identifying variants prone to spontaneous misfolding, which may need close monitoring for the risk of new cervid prion strains emerging, our results highlight residues that strongly influence misfolding resistance. Although these residues may affect spontaneous misfolding differently than known CWD strains propagation, PMSA could pinpoint amino acids with the highest impact, with those reducing spontaneous misfolding as promising candidates for enhancing CWD resistance. Moreover, recent insights into the structure of NA CWD prions underscore the value of our findings. For instance, several residues that lower spontaneous misfolding propensity align with key regions of the prion monomer, such as the polymorphism A136V, located in the E motif, and the changes Q171R and N173S, present at the inner part of the central strand (Alam et al., 2024).

Finally, through intracerebral inoculation of one representative spontaneously generated PMSA product in transgenic mice expressing bank vole 109I PrP (TgVole 1×) (Fernández-Borges et al., 2017), we demonstrate that these misfolded recombinant proteins are *bona fide* prions, and further confirmed its transmissibility through a second passage in the same model. The spontaneous *in vitro* generation of recombinant *bona fide* cervid prions provides new tools to perform systematic *in vitro* studies and explore the effects of all cervid PrP variants on prion propagation. It will also be useful for studies requiring high amounts of pathological prions in a simple and chemically defined environment, such as structural studies. Additionally, the bioassay of the recombinant prions revealed variable phenotypes, possibly indicative of the propagation of different sub-strains. When the brains of the diseased animals were analyzed after both the first and second passage, animals inoculated with the same PMSA preparation showed slightly different electrophoretic PrP^{res} profiles and heterogeneous histopathological lesion and PrP^{res} deposition patterns. However, the heterogeneity of phenotypes observed in the second passage needs to be interpreted with caution since some of the observed features could be attributed to a minimal component of the spontaneous strain generated in the TgVole 1× model which could have arisen during the first passage (>342dpi). The intense hippocampal vacuolation and astrogliosis as well as the punctate PrP^{res} deposition pattern in the oriens layer could be features of the propagation of this atypical strain, plausible for models with the I109 polymorphism or equivalents (Otero et al., 2019; Vidal et al., 2022). Nonetheless, biochemical analysis ruled out the presence of an atypical PK resistant component in these brains, of the characteristic low molecular weight single banded pattern in WB analysis supporting the sub-strains hypothesis. Moreover, the intense vacuolation observed in the striatum region is a feature previously observed in other PMSA generated prion bioassays, and it has been associated with those conformers obtained with dextran sulfate as a cofactor (Erana et al., 2023), since *in vitro* misfolded mouse recombinant PrP conformers obtained without this cofactor lacked an involvement of the striatum, when inoculated to TgVole 1× mice (Pérez-Castro et al., 2025). The punctate PrP^{res} immunolabeling pattern observed in the brain stem (thalamus, midbrain and medulla oblongata) of all the animals in the group resembles that of TgVole 1× adapted CWD and seems to be a constant feature in both 1st and 2nd passages of Deer-Dx-D. However, the heterogeneity of other features, such as the presence or absence of plaques in the hippocampus' albeus layer or the presence or absence of a strong

striatal involvement might be indicative of the propagation of different conformers (or sub-strains). Especially, since similar findings have been previously described when PMCA-generated recombinant prions were inoculated into mice (Bistaffa et al., 2019), suggesting that *in vitro* prion misfolding could result mostly in different conformer mixtures. However, this phenomenon is not only restricted to prions generated *in vitro*: mixtures of sub-strains were also found when brain-derived prions were used to infect cell cultures and *vice versa* (Li et al., 2010), and when sporadic CJD prions were inoculated into transgenic mice expressing human PrP (Cassard et al., 2020). Similarly to the last example and resembling our spontaneously misfolded Q226Q-variant recombinant prion, one of the Nordic moose CWD strains with a possible spontaneous origin has already been characterized, showing at least two different sub-strains that could be distinguished only after transmission into Gt mice expressing cervid PrP (Sun et al., 2023). The concept of prion strains being composed of multiple sub-strains is not new (Collinge and Clarke, 2007), and the selection/adaptation of some sub-strains over others through their transmission into animal models has led to a better understanding of prion strains and to the establishment of some well-known strains (Block and Bartz, 2023). However, this phenomenon is especially notable in CWD, where not only some the new Nordic strains seem to be composed of sub-strains, but also the well-established NA CWD seems to be a cloud of quasi-species, expressing different disease phenotypes depending on the genotype of the host (Bian, 2019). Nevertheless, NA CWD has evolved into a stable strain through its propagation over the years, while those theoretically spontaneous, Nordic CWD strains are highly unstable and have the potential to evolve after their transmission into new hosts (Bian, 2019; Bian et al., 2021), resembling our spontaneously generated recombinant prions. The fact that the different disease phenotypes induced by our recombinant cervid prion differ from any other CWD phenotype reported to date, implies that the cervid reference sequence (Q226Q) can adopt multiple possible prion conformations, each leading to distinct disease phenotypes, and that only a few of them have been observed in nature so far in the forms of NA CWD and the Nordic CWD strains. This consideration applies to the cervid reference sequence, just one of the multiple variants of the cervid PrP, but we have shown that most of them have a high propensity to spontaneously misfold. This fact implies that, if they behave in a similar way than Q226Q variant, the spontaneous misfolding of each one of these variants could lead to a plethora of different CWD strains. For that reason, in the current situation where different foci of potential spontaneous CWD have emerged in the Nordic region of Europe, further studies focusing on the relationship between cervid PrP genotypes, and the emergence of different strains could provide valuable insights into the future of CWD. While our findings demonstrate that flexibility, thermostability, and spontaneous misfolding propensity function as largely independent parameters in cervid PrP variants, the applicability of these observations to other mammalian prion proteins, particularly human PrP, requires further investigation. Human genetic prion diseases exhibit variable disease onset and progression that may involve additional factors such as strain-specific propagation mechanisms, cellular stress responses, and species-specific protein-cofactor interactions that differ from the spontaneous misfolding processes examined in this study. The sequence differences between human and cervid PrP, distinct post-translational modifications, and different cellular environments may significantly influence the relationship between protein flexibility and disease pathogenesis. Future comparative studies examining flexibility-misfolding relationships across different mammalian PrP sequences, including human variants associated with genetic prion diseases, would be valuable to determine the broader applicability of our findings and their relevance to understanding human prion disease mechanisms.

Overall, the evaluation of the spontaneous misfolding propensity of all cervid PrP variants using PMSA, combined with T_m measurements and *in silico* estimation of flexibility of the globular isoforms, indicates a lack of correlation between these parameters (Fig. 6). This suggests that other, yet unknown factors may determine the spontaneous misfolding capacity of each PrP variant. Our PMSA assay enabled us to identify polymorphic hotspots with a major influence on misfolding susceptibility or resistance. Additionally, the study generated a set of *bona fide* recombinant cervid prions for future research, not only on spontaneous misfolding but also on prion propagation and strain variation across different cervid species.

5. Conclusions

Our findings highlight the complexity of spontaneous PrP misfolding, showing that factors beyond thermostability and structural flexibility are likely involved. This suggests that these three parameters are unrelated, addressing the debate over their potential correlation in neurodegenerative diseases associated with protein misfolding, such as Alzheimer's and Parkinson's. By identifying cervid PrP polymorphic residues that strongly influence misfolding susceptibility or resistance, this study provides new insights into the structural features that drive prion conversion and highlights the potential risk of certain variants in the emergence of new CWD outbreaks.

Supplementary data to this article can be found online at https://doi.org/10.1016/j.nbd.2025.107005.

Declaration of generative AI and AI-assisted technologies

All the cervid images used in the PrPdex files presented in this article and available in the website https://prpdex.com/cervidae/ were generated using the DALL-E3 model as implemented in GPT-4o. After using this tool or service, the corresponding author reviewed and edited the content as needed and takes full responsibility for the content of the publication.

CRediT authorship contribution statement

Carlos M. Díaz-Domínguez: Writing – review & editing, Writing – original draft, Visualization, Validation, Methodology, Investigation, Formal analysis, Data curation, Conceptualization. **Hasier Eraña:** Writing – review & editing, Project administration, Methodology, Investigation, Conceptualization. **Francesca Peccati:** Writing – review & editing, Writing – original draft, Software, Investigation, Data curation, Conceptualization. **Enric Vidal:** Writing – review & editing, Visualization, Supervision, Formal analysis. **Jorge M. Charco:** Writing – review & editing, Supervision, Investigation. **Cristina Sampedro-Torres-Quevedo:** Writing – review & editing, Investigation. **Miguel A. Pérez-Castro:** Writing – review & editing, Investigation. **Nuria L. Lorenzo:** Writing – review & editing, Investigation. **Samanta Giler:** Writing – review & editing, Formal analysis. **Glenn C. Telling:** Writing – review & editing, Resources. **Mariví Geijo:** Writing – review & editing, Validation, Supervision, Resources. **Jesús R. Requena:** Writing – review & editing, Resources, Investigation. **Gonzalo Jiménez-Osés:** Writing – review & editing, Writing – original draft, Validation, Resources, Project administration, Funding acquisition, Formal analysis, Conceptualization. **Joaquín Castilla:** Writing – review & editing, Supervision, Resources, Project administration, Funding acquisition, Conceptualization.

Ethics approval and consent to participate

TgVole 1× (FVB/N.129Ola-Tg(Prnp-Bvole109I)C594PRC/Cicb) founder mice were generated at Transgenic Facility of the University of Salamanca (Spain) and breeding colonies were kept on a 12:12 light/dark cycle, receiving food and water *ad libitum* at CIC bioGUNE (Spain). TgVole 1× mice inoculated at Neiker - Basque Institute for Agricultural Research and Development and at Centro de Biomedicina Experimental (CEBEGA) - University of Santiago de Compostela, registered in the Spanish Register of breeding, supplier and user centers with the number ES150780292901. All experiments adhered to the guidelines outlined in the Spanish law "Real Decreto 53/2013 de 1 de febrero" on the

protection of animals used for experimentation and other scientific purposes, based on the European Directive 2010/63/UE on Laboratory Animal Protection. The project received approval from the Ethical Committees on Animal Welfare (project code P-CBG-CBBA-0519 at CIC bioGUNE, NEIKER-OEBA-2021-003 at Neiker, with the authorisation DFB/BFA 2021/49 of the Competent Authority, Diputación Foral de Bizkaia, and permit 15,005/16/006 at CEBEGA) and was conducted under their supervision.

Funding

The present work was partially funded by three different grants awarded by "Agencia Estatal de Investigación, Ministerio de Ciencia e Innovación" (Spanish Government), grant numbers PID2021-122201OB-C21, PID2021-1222010B-C22, and PID2020-117465GB-I00, funded by MCIN/AEI /10.13039/501100011033 and co-financed by the European Regional Development Fund (ERDF). Also funded by MCIN/AEI /10.13039/501100011033, F.P. and G.J.O. were provided with the grants RYC2022-036457-I and PID2021-125946OB-I00, respectively. EFA031/01 NEURO-COOP, which is co-funded at 65 % by the European Union through Programa Interreg VI-A España-Francia-Andorra (POCTEFA 2021-2027). Additional funding was provided by the Instituto de Salud Carlos III (ISCIII), grant number AC21_2/00024, as part of a grant from the European Joint Program for Neurodegenerative Research (JPND) JPND-2021-650-130. Additionally, CIC bioGUNE currently holds a Severo Ochoa Excellence accreditation, CEX2021-001136-S, also funded by MCIN/AEI /10.13039/501100011033. The funders had no role in study design, data collection and analysis, decision to publish, or preparation of the manuscript.

Declaration of competing interest

Authors have read the journal's policy and have the following competing interests to declare: Authors Hasier Eraña and Jorge M. Charco are employed by the commercial company ATLAS Molecular Pharma SL. This does not alter our adherence to all Journal policies on sharing data and materials and did not influence in any way the work reported in this manuscript.

Acknowledgments

The authors would like to thank the following for their support: Ikerbasque foundation, vivarium, maintenance, IT and Electron Microscopy Platform from CIC bioGUNE for outstanding assistance; Maria de la Sierra Espinar and the rest of the personnel from CReSA for the technical support; and Neiker and CEBEGA's biocontainment unit staff for excellent care and maintenance of the animals; César P. Díaz Domínguez for his invaluable contribution through the generation of cervid images for the manuscript. The authors would also like to acknowledge the work from past laboratory members of the Prion Research Lab from CIC bioGUNE, that despite not being directly involved in the manuscript have contributed along the years to the development of all the methods and techniques currently used in the laboratory.

Data availability

All data generated or analyzed during this study are included in this published article (and its supplementary information files).

All detailed information for each variant analyzed in this study is compiled in PrPdex files which can be accessed at https://prpdex.com/cervidae/.

References

Alam, P., et al., 2024. Cryo-EM structure of a natural prion: chronic wasting disease fibrils from deer. Acta Neuropathol. 148, 56.
Andersen, H.C., 1980. Molecular dynamics simulations at constant pressure and/or temperature. J. Chem. Phys. 72, 2384–2393.
Angers, R., et al., 2014. Structural Effects of PrP Polymorphisms on Intra- and Interspecies Prion Transmission Proceedings of the National Academy of Sciences.
Arifin, M.I., et al., 2020. Large-scale prion protein genotyping in Canadian caribou populations and potential impact on chronic wasting disease susceptibility. Mol. Ecol. 29, 3830–3840.
Arifin, M.I., et al., 2021. Cervid prion protein polymorphisms: role in chronic wasting disease pathogenesis. Int. J. Mol. Sci. 22, 2271.
Arifin, M.I., et al., 2023. Heterozygosity for cervid S138N polymorphism results in subclinical CWD in gene-targeted mice and progressive inhibition of prion conversion. Proc. Natl. Acad. Sci. USA 120, e2221060120.
Arifin, M.I., et al., 2024. Norwegian moose CWD induces clinical disease and neuroinvasion in gene-targeted mice expressing cervid S138N prion protein. PLoS Pathog. 20, e1012350.
Bartz, J.C., et al., 2024. Chronic wasting disease: state of the science. Pathogens 13.
Benestad, S.L., Telling, G.C., 2018. Chronic wasting disease: an evolving prion disease of cervids. Handb. Clin. Neurol. 153, 135–151.
Benestad, S.L., et al., 2003. Cases of scrapie with unusual features in Norway and designation of a new type, Nor98. Vet. Rec. 153, 202–208.
Benestad, S.L., et al., 2016. First case of chronic wasting disease in Europe in a Norwegian free-ranging reindeer. Vet. Res. 47, 88.
Bett, C., et al., 2012. Structure of the beta2-alpha2 loop and interspecies prion transmission. FASEB J. 26, 2868–2876.
Bian, B., et al., 2019. Primary structural differences at residue 226 of deer and elk PrP dictate selection of distinct CWD prion strains in gene-targeted mice. Proc. Natl. Acad. Sci. 116 (25), 12478–12487.
Bian, J., et al., 2021. Adaptive selection of a prion strain conformer corresponding to established north American CWD during propagation of novel emergent Norwegian strains in mice expressing elk or deer prion protein. PLoS Pathog. 17, e1009748.
Bistaffa, E., et al., 2019. Synthetic prion selection and adaptation. Mol. Neurobiol. 56, 2978–2989.
Block, A.J., Bartz, J.C., 2023. Prion strains: shining new light on old concepts. Cell Tissue Res. 392, 113–133.
Brandt, A.L., et al., 2015. Prion protein gene sequence and chronic wasting disease susceptibility in white-tailed deer (Odocoileus virginianus). Prion 9, 449–462.
Brayton, K.A., et al., 2004. A processed pseudogene contributes to apparent mule deer prion gene heterogeneity. Gene 326, 167–173.
Buchholz, M.J., et al., 2021. Characterization of the prion protein gene in axis deer (Axis axis) and implications for susceptibility to chronic wasting disease. Prion 15, 44–52.
Case, D.A., et al., 2023. AmberTools. J. Chem. Inf. Model. 63, 6183–6191.
Cassard, H., et al., 2020. Prions from sporadic Creutzfeldt-Jakob disease patients propagate as strain mixtures. mBio 11 e00393-20.
Cervenakova, L., et al., 1997. High sequence homology of the PrP gene in mule deer and Rocky Mountain elk. Lancet 350, 219–220.
Colby, D.W., Prusiner, S.B., 2011. Prions. Cold Spring Harb. Perspect. Biol. 3, 1–22.
Collinge, J., 2001. Prion diseases of humans and animals: their causes and molecular basis. Annu. Rev. Neurosci. 24, 519–550.
Collinge, J., Clarke, A.R., 2007. A general model of prion strains and their pathogenicity. Science 318, 930–936.
Cullingham, C.I., et al., 2020. Predicting the spread-risk potential of chronic wasting disease to sympatric ungulate species. Prion 14, 56–66.
Curcio, L., et al., 2016. Review: a review on classical and atypical scrapie in caprine: prion protein gene polymorphisms and their role in the disease. Animal 10, 1585–1593.
Darden, T., et al., 1993. Particle mesh Ewald: an N·log(N) method for Ewald sums in large systems. J. Chem. Phys. 98, 10089–10092.
Erana, H., et al., 2019. Development of a new largely scalable in vitro prion propagation method for the production of infectious recombinant prions for high resolution structural studies. PLoS Pathog. 15, e1008117.
Erana, H., et al., 2023. Understanding the key features of the spontaneous formation of bona fide prions through a novel methodology that enables their swift and consistent generation. Acta Neuropathol. Commun. 11, 145.
Eraña, H., et al., 2023. Understanding the key features of the spontaneous formation of bona fide prions through a novel methodology that enables their swift and consistent generation. Acta Neuropathol. Commun. 11.
Erana, H., et al., 2024. A protein Misfolding shaking amplification-based method for the spontaneous generation of hundreds of bona fide prions. Nat. Commun. 15, 2112.
Farre, M., et al., 2019. An integrated chromosome-scale genome assembly of the Masai giraffe (Giraffa camelopardalis tippelskirchi). Gigascience 8.
Fernández-Borges, N., et al., 2017. Cofactors influence the biological properties of infectious recombinant prions. Acta Neuropathol. 135 (2), 179–199.
Fox, K.A., et al., 2006. Patterns of PrPCWD accumulation during the course of chronic wasting disease infection in orally inoculated mule deer (Odocoileus hemionus). J. Gen. Virol. 87, 3451–3461.
Green, K.M., et al., 2008. The elk PRNP codon 132 polymorphism controls cervid and scrapie prion propagation. J. Gen. Virol. 89, 598–608.
Güere, M.E., et al., 2022. Chronic wasting disease in Norway—a survey of prion protein gene variation among cervids. Transbound. Emerg. Dis. 69, e20–e31.
Hamir, A.N., et al., 2006. Transmission of chronic wasting disease of mule deer to Suffolk sheep following intracerebral inoculation. J. Vet. Diagn. Invest. 18, 558–565.
Hannaoui, S., et al., 2017. Destabilizing polymorphism in cervid prion protein hydrophobic core determines prion conformation and conversion efficiency. PLoS Pathog. 13, e1006553.

Hannaoui, S., et al., 2021. New and distinct chronic wasting disease strains associated with cervid polymorphism at codon 116 of the Prnp gene. PLoS Pathog. 17, e1009795.
Happ, G.M., et al., 2007. Prion protein genes in caribou from Alaska. J. Wildl. Dis. 43, 224–228.
Heaton, M.P., et al., 2003. Prion gene sequence variation within diverse groups of U.S. sheep, beef cattle, and deer. Mamm. Genome 14, 765–777.
Hill, A.F., et al., 2003. Molecular classification of sporadic Creutzfeldt-Jakob disease. Brain 126, 1333–1346.
Humphrey, W., et al., 1996. VMD: visual molecular dynamics. J. Mol. Graph. 14 (33–8), 27–28.
Huson, H.J., Happ, G.M., 2006. Polymorphisms of the prion protein gene (PRNP) in Alaskan moose (Alces alces gigas). Anim. Genet. 37, 425–426.
Ishida, Y., et al., 2020. Association of chronic wasting disease susceptibility with prion protein variation in white-tailed deer (Odocoileus virginianus). Prion 14, 214–225.
Izadi, S., Onufriev, A.V., 2016. Accuracy limit of rigid 3-point water models. J. Chem. Phys. 145, 074501.
Jeong, H.J., et al., 2007. Identification of single-nucleotide polymorphisms of the prion protein gene in sika deer (Cervus nippon laiouanus). J. Vet. Sci. 8, 299–301.
Johnson, C., et al., 2003. Prion protein gene heterogeneity in free-ranging white-tailed deer within the chronic wasting disease affected region of Wisconsin. J. Wildl. Dis. 39, 576–581.
Johnson, C.J., et al., 2011. Prion protein polymorphisms affect chronic wasting disease progression. PLoS One 6, e17450.
Jumper, J., et al., 2021. Highly accurate protein structure prediction with AlphaFold. Nature 596, 583–589.
Kaluz, S., et al., 1997. Sequencing analysis of prion genes from red deer and camel. Gene 199, 283–286.
Kim, J.I., et al., 2010. Mammalian prions generated from bacterially expressed prion protein in the absence of any mammalian cofactors. J. Biol. Chem. 285, 14083–14087.
Kotov, V., et al., 2021. In-depth interrogation of protein thermal unfolding data with MoltenProt. Protein Sci. 30, 201–217.
Li, J., et al., 2010. Darwinian evolution of prions in cell culture. Science 327, 869–872.
Li, P., et al., 2015. Systematic parameterization of monovalent ions employing the nonbonded model. J. Chem. Theory Comput. 11, 1645–1657.
Meyerett-Reid, C., et al., 2017. De novo generation of a unique cervid prion strain using protein misfolding cyclic amplification. mSphere 2 e00372–16.
Miller, W.L., Walter, W.D., 2020. Can genetic assignment tests provide insight on the influence of captive egression on the epizootiology of chronic wasting disease? Evol. Appl. 13, 715–726.
Miyamoto, S., Kollman, P.A., 1992. Settle: an analytical version of the SHAKE and RATTLE algorithm for rigid water models. J. Comput. Chem. 13, 952–962.
Moore, J., et al., 2020. Novel strain of the chronic wasting disease agent isolated from experimentally inoculated elk with LL132 prion protein. Sci. Rep. 10.
Moreno, J.A., Telling, G.C., 2018. Molecular mechanisms of chronic wasting disease prion propagation. Cold Spring Harb. Perspect. Med. 8.
Nalls, A.V., et al., 2013. Mother to offspring transmission of chronic wasting disease in reeves' Muntjac deer. PLoS One 8.
Nonno, R., et al., 2020. Studies in bank voles reveal strain differences between chronic wasting disease prions from Norway and North America. Proc. Natl. Acad. Sci. USA 117, 31417–31426.
O'Rourke, K.I., et al., 1998. Monoclonal antibody F89/160.1.5 defines a conserved epitope on the ruminant prion protein. J. Clin. Microbiol. 36, 1750–1755.
Otero, A., et al., 2019. A single amino acid substitution, found in mammals with low susceptibility to prion diseases, delays propagation of two prion strains in highly susceptible transgenic mouse models. Mol. Neurobiol. 56 (9), 6501–6511.
Otero, A., et al., 2023. Emergence of CWD strains. Cell Tissue Res. 392, 135–148.
Ott-Conn, C.N., et al., 2021. Prion protein polymorphisms in Michigan white-tailed deer (Odocoileus virginianus). Prion 15, 183–190.
Peletto, S., et al., 2009. Genetic variability of the prion protein gene (PRNP) in wild ruminants from Italy and Scotland. J. Vet. Sci. 10, 115–120.
Pérez-Castro, M.A., et al., 2025. Cofactors facilitate bona fide prion misfolding in vitro but are not necessary for the infectivity of recombinant murine prions. PLoS Pathog. 21 (1), e1012890.
Perrin-Stowe, T.I.N., et al., 2020. Prion protein gene (PRNP) sequences suggest differing vulnerability to chronic wasting disease for Florida key deer (Odocoileus virginianus clavium) and Columbian white-tailed deer (O. v. Leucurus). J. Hered. 111, 564–572.
Perucchini, M., et al., 2008. PrP genotypes of free-ranging wapiti (Cervus elaphus nelsoni) with chronic wasting disease. J. Gen. Virol. 89, 1324–1328.
Pirisinu, L., et al., 2018. Novel type of chronic wasting disease detected in moose (Alces alces), Norway. Emerg. Infect. Dis. 24, 2210–2218.
Pritzkow, S., et al., 2022. North American and Norwegian chronic wasting disease prions exhibit different potential for interspecies transmission and zoonotic risk. J. Infect. 225 (3), 542–551.
Prusiner, S.B., 1998. Prions. Proc. Natl. Acad. Sci. USA 95, 13363–13383.
Raymond, G.J., et al., 2000. Evidence of a molecular barrier limiting susceptibility of humans, cattle and sheep to chronic wasting disease. EMBO J. 19, 4425–4430.
Rhyan, J.C., et al., 2011. Failure of fallow deer (Dama dama) to develop chronic wasting disease when exposed to a contaminated environment and infected mule deer (Odocoileus hemionus). J. Wildl. Dis. 47, 739–744.
Robinson, S.J., et al., 2012. The role of genetics in chronic wasting disease of north American cervids. Prion 6, 153–162.
Robinson, A.L., et al., 2019. Variation in the prion protein gene (PRNP) sequence of wild deer in Great Britain and mainland Europe. Vet. Res. 50, 59.
Rodríguez-Martínez, A.B., et al., 2010. Atypical/Nor98 scrapie in the Basque Country: a case report of eight outbreaks. BMC Vet. Res. 6.
Roe, D.R., Cheatham 3rd, T.E., 2013. PTRAJ and CPPTRAJ: software for processing and analysis of molecular dynamics trajectory data. J. Chem. Theory Comput. 9, 3084–3095.
Roh, I.S., et al., 2020. Identification of the prion-related protein gene (PRNT) sequences in various species of the Cervidae family. Mol. Biol. Rep. 47, 6155–6164.
Saa, P., et al., 2005. Cyclic amplification of protein misfolding and aggregation. Methods Mol. Biol. 299, 53–65.
Schatzl, H.M., et al., 1997. Is codon 129 of prion protein polymorphic in human beings but not in animals? Lancet 349, 1603–1604.
Scott, M., et al., 1993. Propagation of prions with artificial properties in transgenic mice expressing chimeric PrP genes. Cell 73, 979–988.
Siso, S., et al., 2004. Distribution of PrP(res) in the brains of BSE-affected cows detected by active surveillance in Catalonia, Spain. Vet. Rec. 155, 524–525.
Smits, M.A., et al., 1997. Prion protein and scrapie susceptibility. Vet. Q. 19, 101–105.
Sola, D., et al., 2023. Heterogeneity of pathological prion protein accumulation in the brain of moose (Alces alces) from Norway, Sweden and Finland with chronic wasting disease. Vet. Res. 54, 74.
Sun, J.L., et al., 2023. Novel prion strain as cause of chronic wasting disease in a moose, Finland. Emerg. Infect. Dis. 29, 323–332.
Terry, C., et al., 2019. Structural features distinguishing infectious ex vivo mammalian prions from non-infectious fibrillar assemblies generated in vitro. Sci. Rep. 9, 376.
Tian, C., et al., 2020. ff19SB: amino-acid-specific protein backbone parameters trained against quantum mechanics energy surfaces in solution. J. Chem. Theory Comput. 16, 528–552.
Tranulis, M., et al., 2021. Chronic wasting disease in Europe: new strains on the horizon. Acta Vet. Brno. Scand. 63 (1), 48.
Vázquez-Miranda, H., Zink, R.M., 2020. Geographic distribution of chronic wasting disease resistant alleles in Nebraska, with comments on the evolution of resistance. J. Fish Wildl. Manag. 11, 46–55.
Vidal, E., et al., 2015. Transgenic mouse bioassay: evidence that rabbits are susceptible to a variety of prion isolates. PLoS Pathog. 11, e1004977.
Vidal, E., et al., 2022. Bona fide atypical scrapie faithfully reproduced for the first time in a rodent model. Acta Neuropathol. Commun. 10, 179.
Vikoren, T., et al., 2019. First detection of chronic wasting disease in a wild Red Deer (Cervus elaphus) in Europe. J. Wildl. Dis. 55, 970–972.
Weissmann, C., 2004. The state of the prion. Nat. Rev. Microbiol. 2, 861–871.
Wik, L., et al., 2012. Polymorphisms and variants in the prion protein sequence of European moose (Alces alces), reindeer (Rangifer tarandus), roe deer (Capreolus capreolus) and fallow deer (Dama dama) in Scandinavia. Prion 6, 256–260.
Wilson, G.A., et al., 2009. Polymorphisms at the PRNP gene influence susceptibility to chronic wasting disease in two species of deer (Odocoileus Spp.) in western Canada. J. Toxicol. Environ. Health A 72, 1025–1029.
Wright, T.A., et al., 2017. Extraction of thermodynamic parameters of protein unfolding using parallelized differential scanning Fluorimetry. J. Phys. Chem. Lett. 8, 553–558.
Zink, R.M., et al., 2020. Geographic variation in the PRNP gene and its promoter, and their relationship to chronic wasting disease in north American deer. Prion 14, 185–192.